Solar Phys (2011) 272:159–188
DOI 10.1007/s11207-011-9808-4

Solar Spectral Irradiance Variations in 240 – 1600 nm During the Recent Solar Cycles 21 – 23

J. Pagaran · M. Weber · M.T. DeLand · L.E. Floyd · J.P. Burrows

Received: 7 February 2011 / Accepted: 25 May 2011 / Published online: 12 July 2011

Abstract Regular solar spectral irradiance (SSI) observations from space that simultaneously cover the UV, visible (vis), and the near-IR (NIR) spectral region began with SCIAMACHY aboard ENVISAT in August 2002. Up to now, these direct observations cover less than a decade. In order for these SSI measurements to be useful in assessing the role of the Sun in climate change, records covering more than an eleven-year solar cycle are required. By using our recently developed empirical SCIA proxy model, we reconstruct daily SSI values over several decades by using solar proxies scaled to short-term SCIAMACHY solar irradiance observations to describe decadal irradiance changes. These calculations are compared to existing solar data: the UV data from SUSIM/UARS, from the DeLand & Cebula satellite composite, and the SIP model (S2K+VUV2002); and UV-vis-IR data from the NRLSSI and SATIRE models, and SIM/SORCE measurements. The mean SSI of the latter models show good agreement (less than 5%) in the vis regions over three decades while larger disagreements (10 – 20%) are found in the UV and IR regions. Between minima and maxima of Solar Cycles 21, 22, and 23, the inferred SSI variability from the SCIA proxy is intermediate between SATIRE and NRLSSI in the UV. While the DeLand & Cebula composite provide the highest variability between solar minimum and maximum, the SIP/Solar2000 and NRLSSI models show minimum variability, which may be due to the use of a single proxy in the modeling of the irradiances. In the vis-IR spectral region, the

J. Pagaran (✉) · M. Weber · J.P. Burrows
Institute of Environmental Physics (IUP), Department of Physics and Engineering, University of Bremen, Bremen, Germany
e-mail: pagaran@iup.physik.uni-bremen.de

M. Weber
e-mail: weber@uni-bremen.de

M.T. DeLand
Science System and Applications, Inc (SSAI), Lanham, MD, USA
e-mail: matthew.deland@ssaihq.com

L.E. Floyd
Interferometrics Inc., Herndon, VA, USA
e-mail: floyd@interf.com

SCIA proxy model reports lower values in the changes from solar maximum to minimum, which may be attributed to overestimations of the sunspot proxy used in modeling the SCIAMACHY irradiances. The fairly short timeseries of SIM/SORCE shows a steeper decreasing (increasing) trend in the UV (vis) than the other data during the descending phase of Solar Cycle 23. Though considered to be only provisional, the opposite trend seen in the visible SIM data challenges the validity of proxy-based linear extrapolation commonly used in reconstructing past irradiances.

Keywords Solar irradiance · Solar cycle, models · Solar cycle, observations · Active regions · Sunspots

1. Introduction

There is a high demand to have SSI (solar spectral irradiance) measurements from space that not only cover a spectral range from the UV to the vis-IR (visible-infrared) but also are available over a relatively long time span of several decades (Fröhlich and Lean, 2004; Thuillier *et al.*, 2004; Rottman, 2006; Domingo *et al.*, 2009). Apart from the potential to provide a solar – stellar astrophysical connection (see, for example, Beasley and Cram, 1990), such a long-term archive of SSI data is a key in understanding the solar-terrestrial relations, in particular the extent to which changes in spectral regions of the Sun's radiative output can influence the behavior of the Earth's climate system (see, for example, Arnold, 2002; Fröhlich and Lean, 2004; Haigh, 2007; de Wit and Watermann, 2010; Gray *et al.*, 2010).

Addressing this demand has its intrinsic difficulties (Bonnet, 1981). Notably, operating a space instrument has to be stable and accurately calibrated. In addition, the instrument has to be sensitive to the desired magnitude of variability at the required spectral region. While the UV variations are large, the vis-IR variations are tiny and vary between about 0.2% and 0.4% (see, *e.g.*, Pagaran, Weber, and Burrows, 2009). Hence, for a detector to observe these tiny variations, it has to have a relative uncertainty of a few parts in 10^4 over its lifetime (Rottman *et al.*, 1998). The lifetime of a single instrument is typically 5 – 10 years. In order to observe SSI variability on 11-year solar cycle timescales and longer, these measurements have to originate from several instruments, each with well-calibrated optical elements, including proper correction of instrument degradation over the timescale of interest and biases between instruments.

Regular space-borne irradiance monitoring from several instruments started in 1978 (start of satellite era). The wavelength coverage in early satellite SSI measurements were limited to the UV below 400 nm. This irradiance record provided the opportunity to develop a UV composite (DeLand and Cebula, 2008) by merging independent measurements into one timeseries. Developing a similar composite that includes the vis-IR region (Thuillier *et al.*, 2004) is challenging, as regular measurements in the long wavelength regions started not before the early 2000s. Daily monitoring of the vis-IR started with limited wavelength bands, *e.g.*, SPM of VIRGO/SOHO and with instruments like GOME/ERS-2 and SCIAMACHY/ENVISAT that lack sophisticated in-flight calibration mechanism as it is not required for terrestrial atmospheric observations, the primary purpose of GOME and SCIAMACHY.

The following data are available in the optical spectral range: UV-vis-NIR irradiance data from GOME (Burrows *et al.*, 1999; Weber, Burrows, and Cebula, 1998) since 1995, vis-NIR-SWIR data from SCIAMACHY (Bovensmann *et al.*, 1999; Skupin *et al.*, 2005a, 2005b) since 2002. (SWIR stands for shortwave-IR). In a similar spectral range but at a

lower spectral resolution, SIM data (Harder *et al.*, 2005a, 2005b) from 2003 until present are available.

In Pagaran, Weber, and Burrows (2009), we have shown that spectral irradiance variations can be modeled by parametrizing observed irradiances from SCIAMACHY in terms of solar proxies. In this work, we apply this model, which we hereafter refer to as the SCIA proxy, to reconstruct a long time record of UV-vis-NIR SSI extending back to 1947. Here we focus on the reconstruction of Solar Cycles 21 to 23 starting in 1972. In Section 2 we describe the basic features of the SCIA proxy model, and discuss some sample timeseries of SCIA proxy irradiance timeseries covering the three recent solar cycles. In Section 3, we compare SCIA proxy to other SSI data. While some comparisons with other solar data have been done on solar rotational time scales in 2003 and 2004 and during Solar Cycle 23 (Pagaran, Weber, and Burrows, 2009; Pagaran *et al.*, 2011), Section 4 provides a more comprehensive comparison to a far wider variety of solar data (including the DeLand & Cebula UV composite, SUSIM, and SIM measurements) and covering a larger period (1972 – 2008). This is followed by Sections 5 and 6, where results are discussed and summarized, respectively.

2. SCIA Proxy Model

Here we briefly describe our approach to model solar irradiances from SCIAMACHY. The basic idea in modeling the solar irradiance is to parametrize the timeseries of the observed irradiance in terms of solar proxies (Lean *et al.*, 1997, 2005; Pagaran, Weber, and Burrows, 2009). The solar proxies represent facular brightening (mainly UV) and sunspot darkening (mainly vis/IR), which are the main contributions to SSI variations. A multivariate linear regression is performed to determine the regression coefficients of the solar proxies. In addition to the solar proxy terms, piecewise polynomials are used to correct for instrument degradation and for small biases following instrument and platform anomalies (Pagaran, Weber, and Burrows, 2009). The SCIA proxy model is based on SCIAMACHY observations covering solar rotations during 2003 and 2004. The regression coefficients were determined from 240 nm to 1750 nm (SCIAMACHY Channels 1 to 6) in steps of 10 nm (Pagaran, Weber, and Burrows, 2009). Variations in time are provided by the scaled solar proxy timeseries. For more details on SCIAMACHY and the SCIA proxy model, see Pagaran, Weber, and Burrows (2009).

We calculate daily SSI, $I_\lambda(t)$, using the equation

$$I_\lambda(t) = I_{\text{ref}}(\lambda) + \Delta I(\lambda, t). \tag{1}$$

Here, $I_{\text{ref}}(\lambda)$ is the reference spectrum based on a mean ESM diffuser SCIAMACHY observation (see Figure 1) from 4 March 2004 (t_{ref}) that includes a degradation correction using the daily white-light spectrum (WLS) ratios with respect to data at the beginning of the mission (see the Appendix in Pagaran *et al.* (2011)). The daily SSI anomaly is given by

$$\begin{aligned}\Delta I(\lambda, t) &= a_\lambda \Delta P_a(t) + b_\lambda \Delta P_b(t) \\ &= a_\lambda \big[P_a(t) - P_a(t_{\text{ref}})\big] + b_\lambda \big[P_b(t) - P_b(t_{\text{ref}})\big].\end{aligned} \tag{2}$$

To obtain the daily SSI anomaly, $\Delta I(\lambda, t)$, we use the faculae and sunspot regression parameters, a_λ and b_λ, and the daily change of solar proxies $P(t)$ with respect to the date of the SCIAMACHY reference spectrum (t_{ref}): $\Delta P_a(t)$ and $\Delta P_b(t)$. The subscripts

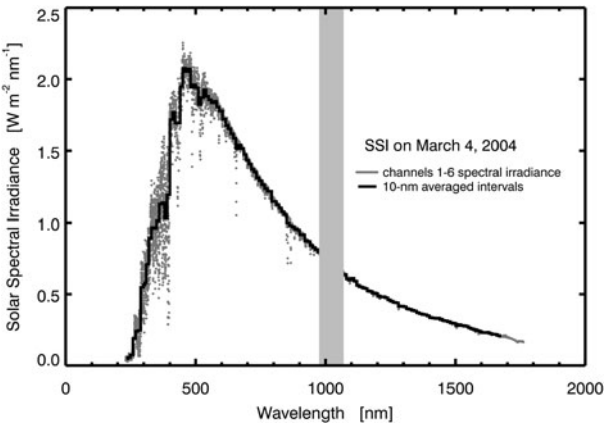

Figure 1 SCIAMACHY reference spectrum $I_{\text{ref}}(\lambda)$ measured on 4th of March 2004. Gray areas (975 – 1070 nm) indicate discarded wavelength regions, *cf.* Pagaran, Weber, and Burrows (2009).

a and b stand for the Mg II core-to-wing (ctw) ratio (Weber, Burrows, and Cebula, 1998; Skupin *et al.*, 2005b; Viereck *et al.*, 2004) and Photometric Sunspot Index (PSI) expressed in fraction of mean TSI (dimensionless) depleted by sunspots (Balmaceda *et al.*, 2009), respectively. The regression parameters have units of irradiance per unit change in the proxy (Pagaran, Weber, and Burrows, 2009), *i.e.*, W m^{-2} nm^{-1} per unit $\Delta P(t)$.

Figure 1 shows the observed reference spectrum, $I_{\text{ref}}(\lambda)$, in its original spectral resolution (gray dots) and binned into 10 nm intervals (solid). The regression parameters, a_λ and b_λ, were determined for the 10 nm bins (Pagaran, Weber, and Burrows, 2009). This 10-nm step binning was applied to all other spectra used in this study.

The uncertainty of $\Delta I_\lambda(t)$ is given by

$$\delta\Delta I(\lambda, t) = \delta a_\lambda \Delta P_a(t) + \delta b_\lambda \Delta P_b(t), \tag{3}$$

with δa_λ and δb_λ being the regression error from fitting to SCIAMACHY observations.

The calculated $I_\lambda(t)$ therefore has wavelength- and time-dependent parts. The time-dependent part is determined by the solar proxies. The top and bottom panels of Figure 2 show Mg II ctw ratio (or $P_a(t)$) and PSI (or $P_b(t)$), respectively. The application of an 81-day smoothing to data points aims at removing the high-frequency signal due to the 27-day solar rotation and enables us to define solar minimum and maximum dates for all solar cycles from the Mg II index timeseries as shown in Figure 2.

We use the recently updated Mg II index, which consists of GOME and SCIAMACHY data (Weber, Burrows, and Cebula, 1998; Skupin *et al.*, 2005b) combined with the multi-satellite composite from Viereck *et al.* (2004). This Mg II composite is extended backwards to 1947 from 1978 using F10.7 cm flux[1] and PSI. The best fit was obtained using the F10.7 cm flux, the square of F10.7 cm flux, and the PSI as fitting terms in a linear regression. The extended Mg II composite correlates also well with UV and EUV wavelengths (Floyd *et al.*, 2005). However, one should keep in mind that the F10.7 cm flux has some deficiencies in modeling UV irradiances (Dudok de Wit *et al.*, 2009a). Viereck *et al.* (2001) showed that Mg II index better tracks EUV changes than F10.7 cm flux, particularly under solar minimum conditions. For reconstructing UV irradiance variations before the satellite era the F10.7 cm flux comes closest to tracking the Mg II index.

[1]The F10.7 cm flux data were taken from the link http://www.oulu.fi/~spaceweb/textbook/f107.html.

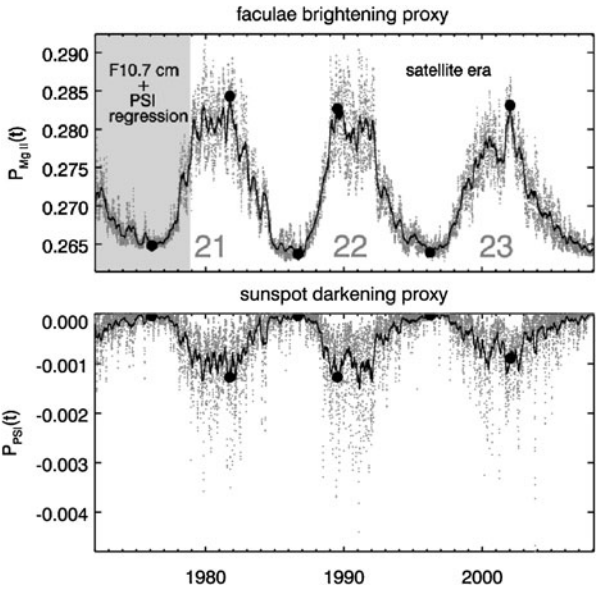

Figure 2 Solar proxy timeseries. Mg II index (top panel) and Photometric Sunspot Index (bottom panel) represent brightening due to faculae and darkening due to sunspots, respectively. The period 1972 to 2008 shown in each panel covers Solar Cycles 21 – 23 with daily (dots) and 81-day smoothed (solid line) values. The solid points indicate maxima and minima (based upon the 81-day smoothed Mg II index timeseries) and define dates of solar maxima and minima used in this study.

Figures 3 and 4 show the reconstructed daily relative SSI variability and its uncertainty (Equations (2) and (3)) in the different spectral regions. The spectral range shown in these figures contains major solar absorption lines, Mg II (279.6 and 280.3 nm), Ca II (393 and 396 nm) doublets; Na I (589 nm), Hα (656 nm); and Ca II triplet (850 and 854 nm), He I multiplet (1083 nm), and the H^- opacity minimum (∼1555 nm).

Across the wavelength range from UV to IR (240 – 1700 nm), the irradiance changes from solar minimum to solar maximum are roughly 7 $\mathrm{mW\,m^{-2}\,nm^{-1}}$ (0.7%) at 380 – 390 nm; it decreases to 1 $\mathrm{mW\,m^{-2}\,nm^{-1}}$ (0.1%) at 655 – 665 nm and 850 – 860 nm and further decreases to 0.2 $\mathrm{mW\,m^{-2}\,nm^{-1}}$ (0.08%) at 1650 – 1660 nm. This observation suggests that $\Delta I\,(\lambda, t)$ reaches maximum at 400 nm before it drops to near zero above 400 nm and then becomes negative at about 1100 nm and 1500 nm. This result is in good qualitative agreement with Figure 2 of Unruh, Solanki, and Fligge (2000). UV irradiance changes are in-phase with solar cycle, while NIR and SWIR are out-of-phase. This observation is similar to Figure 3 of Harder *et al.* (2009), based on Solar Cycle 23 (2004 – 2007) data from SIM (more on this later, *cf.* Figure 18 below).

From the lower subpanels at each wavelength interval shown in Figures 3 and 4 it can be seen that the facular brightening term is the main driver of SSI variability below 400 nm. Above 400 nm, facular brightening and sunspot darkening have opposite signs and nearly cancel each other resulting in nearly zero SSI variability. Above 1000 nm, sunspot darkening becomes the main driver of SSI variability resulting in depleted irradiances at solar maxima. Near the opacity minimum (about 1555 nm) the sunspot darkening term couples with the faculae that also become dark, resulting in a fairly depleted (negative) irradiances at solar maximum. Dark faculae are discussed in Unruh *et al.* (2008) and Pagaran, Weber, and Burrows (2009). Above 1600 nm, facular brightening and sunspot darkening contributions behave like in the vis regions but they are one order of magnitude smaller, *i.e.* 0.1 $\mathrm{mW\,m^{-2}\,nm^{-1}}$ from 1 $\mathrm{mW\,m^{-2}\,nm^{-1}}$ in the vis. Moreover, from these lower subpanels, facular brightening shows a well-defined second maximum in Solar Cycle 23, and a steeper ascending phase in Solar Cycle 22, which is similar in shape to that of the reconstructed Solar Cycle 21.

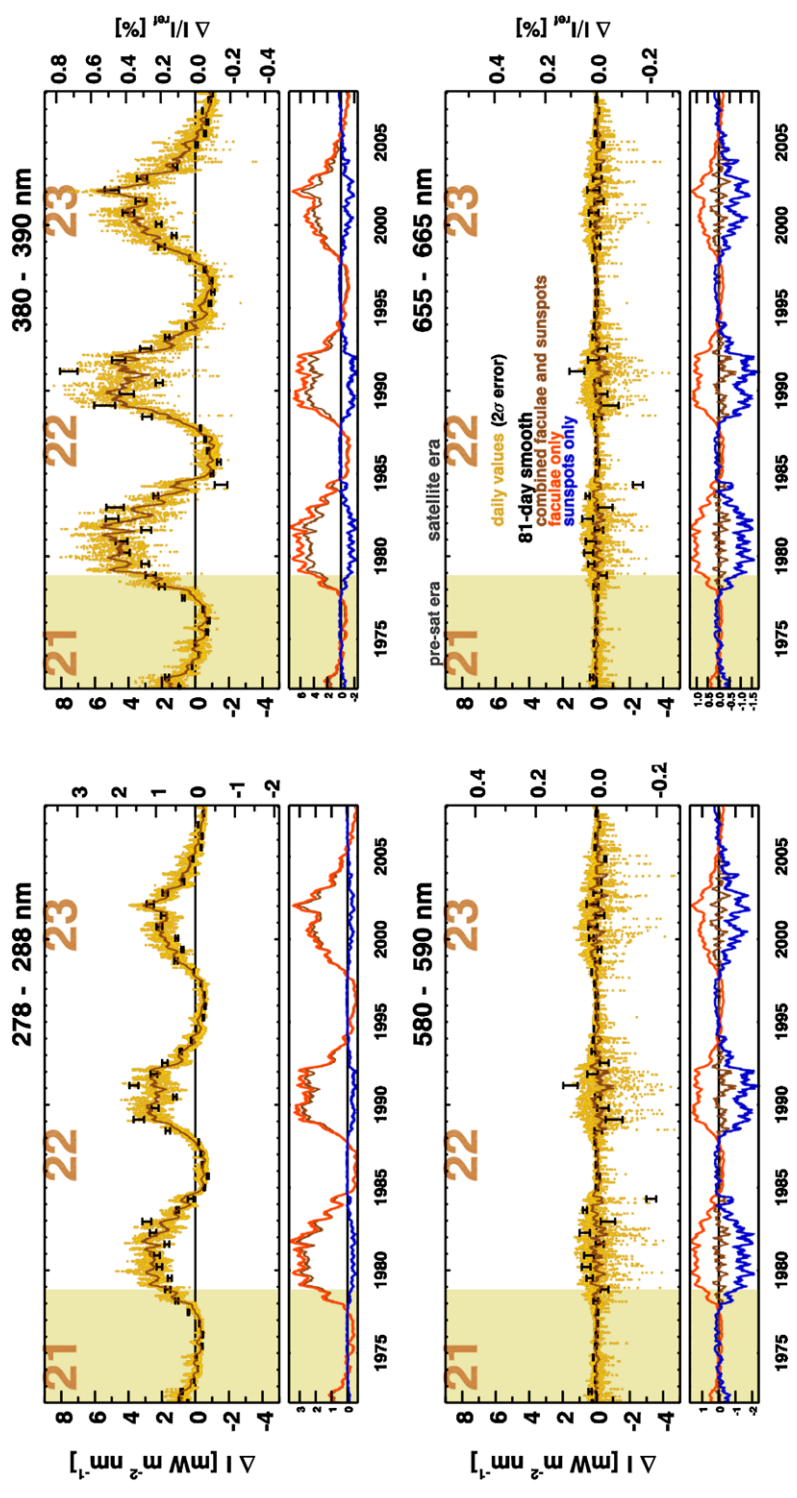

Figure 3 Daily irradiance variability from the SCIA proxy model during 1972 – 2008. Shown are $\Delta I(\lambda, t)$ and $\Delta I(\lambda, t)/I_{\mathrm{ref}}$ on left and right axes, respectively, from selected spectral regions in the UV and vis spectral regions. The upper panels show the daily (golden dots) including their 2σ uncertainty and 81-day smoothed (brown) timeseries from the combined (faculae and sunspots) proxy contributions. The lower small subpanels show the 81-day smoothed faculae (red) and sunspot (blue) contributions, and sum of both (brown).

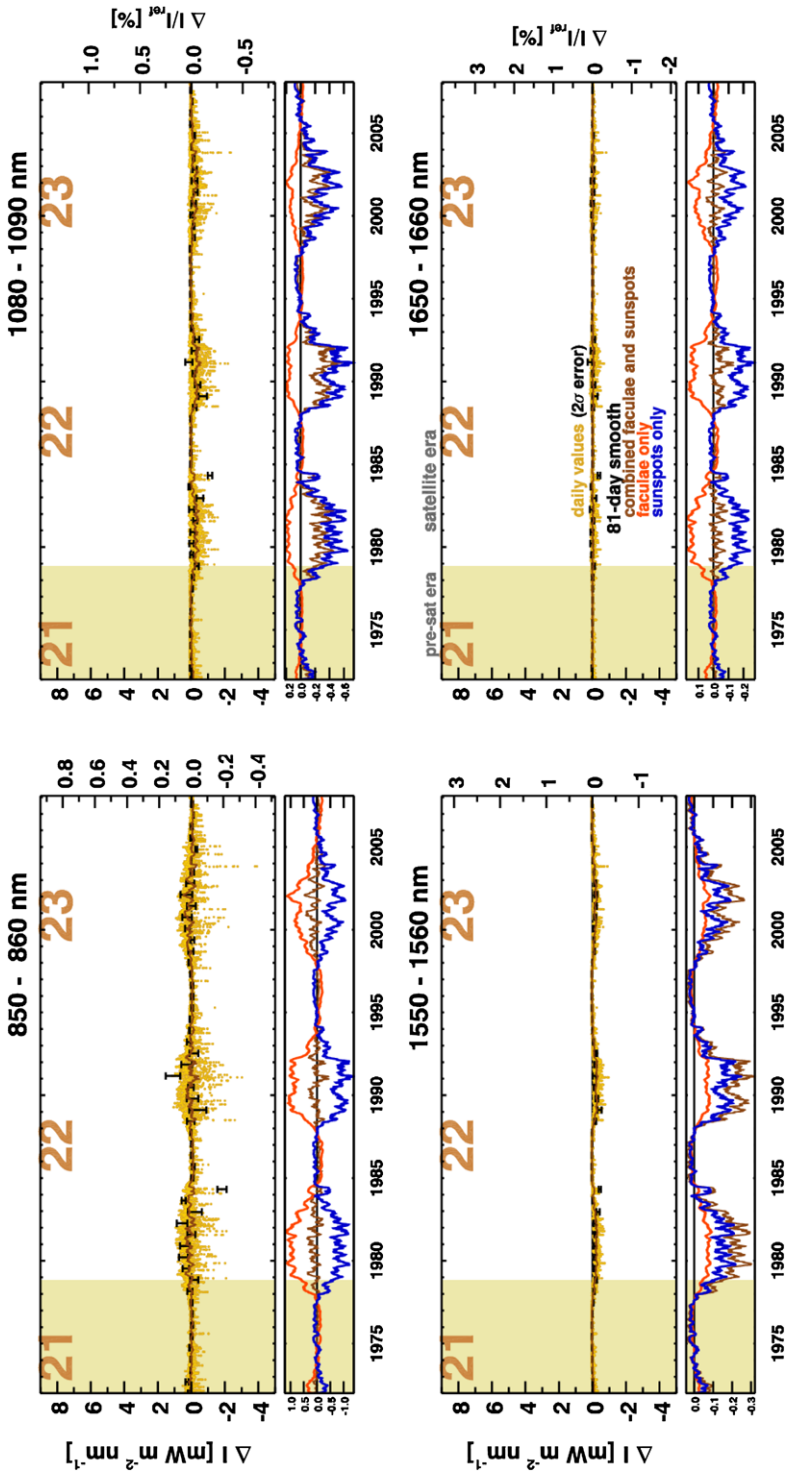

Figure 4 Same as Figure 3 except for showing the NIR and SWIR spectral regions.

Assuming that proxies and SSI behave in similar ways over both 27-day rotational and 11-year solar cycle timescales, changes of solar proxies during the solar cycle and the regression parameters may be used to estimate the 11-year SSI variability on decadal time scales. This assumption is similar to those made in the multi-component proxy-based irradiance models of Lean *et al.* (1997, 2005), DeLand and Cebula (1993), and Woods and Rottman (2002). We will show later that during the short SIM observations period (Harder *et al.*, 2009) this assumption does not hold.

The changes of irradiance from solar minimum (denoted by F_{A}) to solar maximum (denoted by F_{B}) can be estimated as

$$\Delta_{11\mathrm{yr,\,direct}}(\lambda) = 100\frac{\overline{\langle I_\lambda(t_{\mathrm{sol\,max}})\rangle} - \overline{\langle I_\lambda(t_{\mathrm{sol\,min}})\rangle}}{\overline{\langle I_\lambda(t_{\mathrm{sol\,min}})\rangle}} \equiv 100\frac{F_{\mathrm{B}} - F_{\mathrm{A}}}{F_{\mathrm{A}}}. \tag{4}$$

The values for solar cycle variations depend on the choice of dates of solar minima and solar maxima. The solar minima and solar maxima are defined by the extrema of the 81-day smoothed Mg II index. To obtain solar irradiance at solar minimum and solar maximum conditions, the solar irradiances are averaged over 81-days, centered around the extrema dates as indicated in Figure 1 by filled black circles.

The 11-year irradiance variability between solar minimum and solar maximum of Solar Cycles 21 – 23 are shown in Figures 5 – 7, respectively. Faculae contribution during the minimum of Cycle 21 is derived from the extended Mg II index (see Figure 1).

Figure 8 shows a magnified view of the vis-IR SSI variations for Solar Cycles 21 – 23 (including 2σ uncertainty for Cycle 23). Faculae contributions are similar for Cycles 21 – 23 and are almost equal in magnitude. On the other hand, sunspot contributions in Cycle 23 are less negative than in Cycles 21 and 22. For the summed facular and sunspot contributions, Cycle 23 stands out, while Cycle 21 and 22 appear to be similar. The differences of Solar Cycle 23 to the other cycles come, therefore, mainly from the differences in the sunspot darkening term. Between 1400 and 1600 nm both sunspots and faculae become dark (Unruh, Solanki, and Fligge, 1999) and are significantly different from zero for all Solar Cycles 21 to 23.

Lean *et al.* (1997) and Fröhlich and Lean (2004) argue that faculae and sunspots are thought to dominate the long- and short-term irradiance variability, respectively. In the UV, the faculae are the major contributor to SSI variability with sunspot darkening becoming significant in the near UV (300 – 400 nm) (Pagaran, Weber, and Burrows, 2009). In the vis-IR wavelength ranges, faculae and sunspot variations are approximately equal so that they nearly cancel each other. In the spectral region 1200 to 1600 nm, sunspot darkening seems to dominate. These observations are in good qualitative agreement with the findings of Unruh *et al.* (1999, 2008).

3. SSI Observation and Models

A successful irradiance model has to agree with observed irradiance variations as a function of wavelength between solar cycle maximum and minimum (Unruh, Solanki, and Fligge, 1999). Six SSI data sets are used to compare with the SCIA proxy model. Three of them cover only the UV spectral region. They are based on *i*) measurements from SUSIM/UARS (1991 – 2005) (Floyd *et al.*, 2003), *ii*) the SSI composite from DeLand and Cebula (2008), and *iii*) the empirical model from Tobiska *et al.* (2000) or SIP/Solar2000. The remaining three SSI data cover also the vis-IR regions. They are *iv*) the proxy-based model from

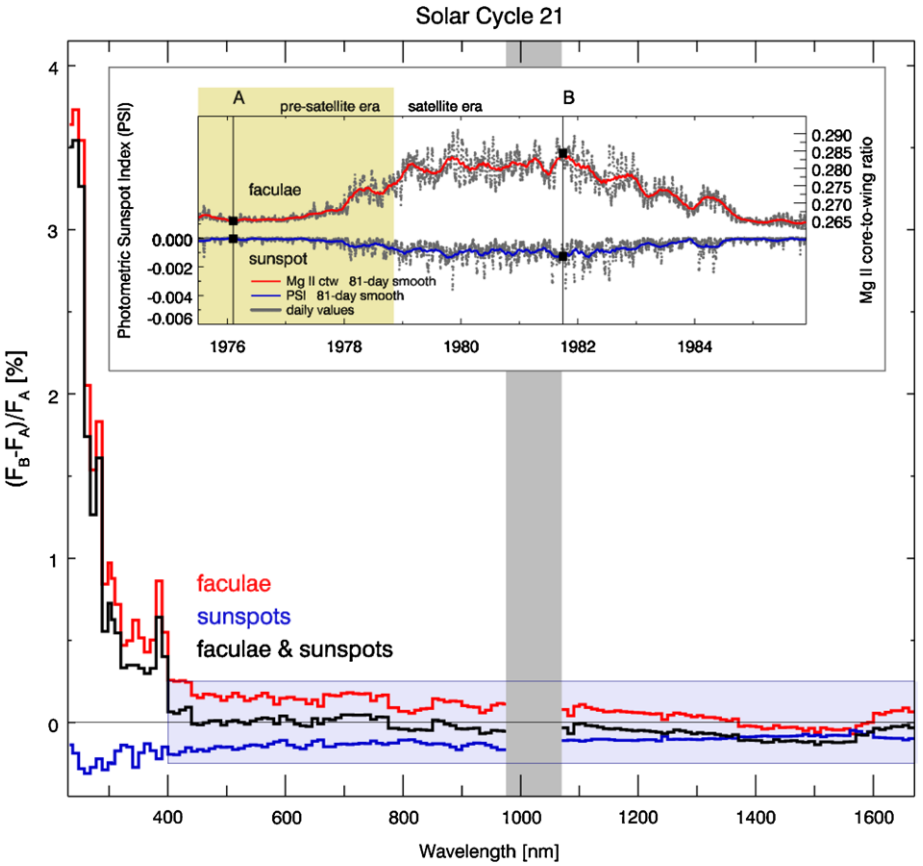

Figure 5 Percent faculae (red) and sunspot (blue) contributions to eleven-year spectral variability (black) between solar minimum and solar maximum of Solar Cycle 21. The scaling factors $\Delta P_a(t)$ and $\Delta P_b(t)$ to scale a_λ and b_λ, respectively, are derived from extrema of 81-day smoothed faculae (inset, top curves) and sunspots (inset, bottom curves) proxy values at F_A and F_B.

NRLSSI (Lean *et al.*, 2005), *v*) the semi-empirical SATIRE model from Krivova *et al.* (2003, 2009, 2011), and *vi*) the measurements from SIM/SORCE (2003 – present) (Harder *et al.*, 2005a, 2005b, 2010). All SSI data are summarized in Table 1.

In the following we briefly describe the various data sets used for comparison.

UV Measurements from SUSIM/UARS or Floyd et al. SUSIM (Solar Ultraviolet Spectral Irradiance Monitor) aboard UARS (*Upper Atmosphere Research Satellite*) is a dual dispersion scanning spectrometer (Brueckner *et al.*, 1993, 1995; Floyd *et al.*, 2003). It measures the full-disk solar ultraviolet spectral irradiance over its 115 – 410 nm wavelength range daily at 1 and 5 nm resolutions and weekly at 0.15 nm resolution. Its daily solar observations began on 11 October 1991 and ended on 1 August 2005.

The data we use here are the daily level 3BS v22 data with a sampling of 1.1 nm.[2] SUSIM covers about 14 years, slightly more than a solar cycle.

[2] http://wwwsolar.nrl.navy.mil/susim_uars_data.html or ftp://ftp.susim.nrl.navy.mil.

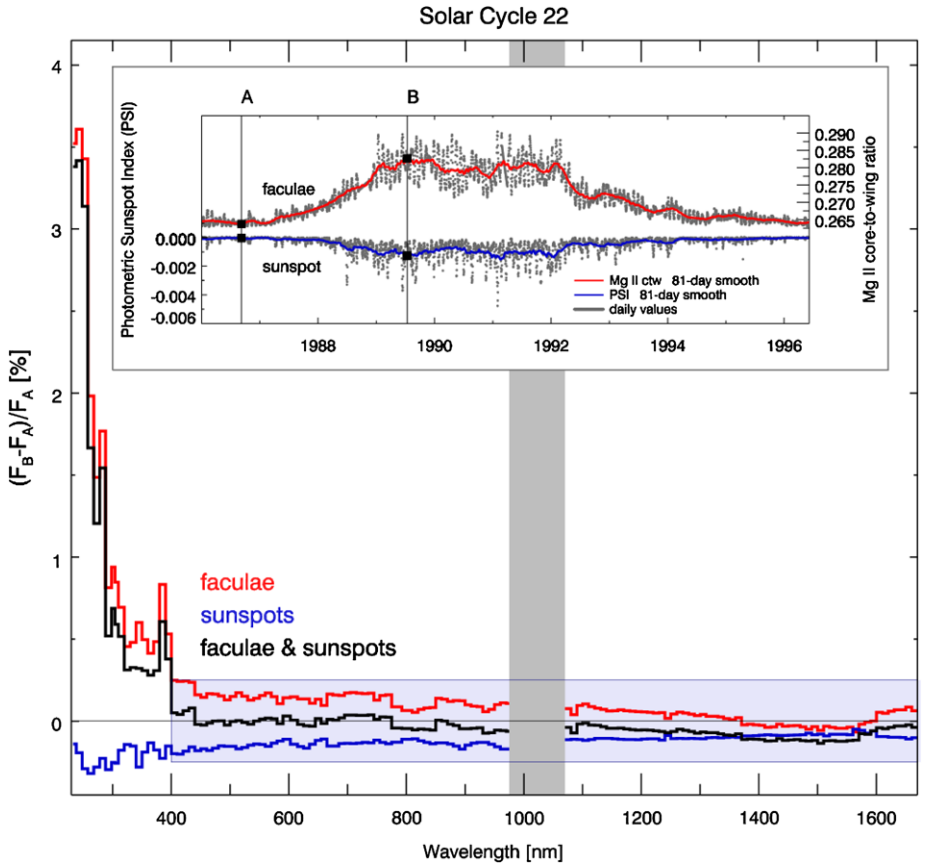

Figure 6 Same as Figure 5 except for Solar Cycle 22.

Table 1 Summary of SSI data used in this study.

Long name	Short name	Spectral coverage	Time coverage	References
Floyd *et al.*	SUSIM	UV	1991 – 2005	Floyd *et al.* (2003)
DeLand & Cebula	SSAI	UV	1978 – 2008	DeLand and Cebula (2008)
Tobiska *et al.*	SIP[a]	UV	1947 – 2052	Tobiska *et al.* (2000)
Lean *et al.* (SSI)	NRLSSI	UV-vis-IR	1950 – 2008	Lean *et al.* (1997, 2005)
Krivova *et al.*	SATIRE	UV-vis-IR	1947 – 2008	Fligge *et al.* (2000)
Harder *et al.*	SIM	UV-vis-IR	2003 – 2009	Harder *et al.* (2005a, 2005b, 2010)
Pagaran *et al.*	SCIA proxy	UV-vis-IR	1947 – 2008	Pagaran *et al.* (2009), & this work

[a]Formerly Solar2000, among the models available we use the S2K+VUV2002 model.

UV Satellite Composite from DeLand & Cebula or SSAI Composite The UV composite (DeLand and Cebula, 2008) or SSAI (Science Systems and Applications, Inc.) was created by merging available UV irradiances from six different space-borne instruments, SME,

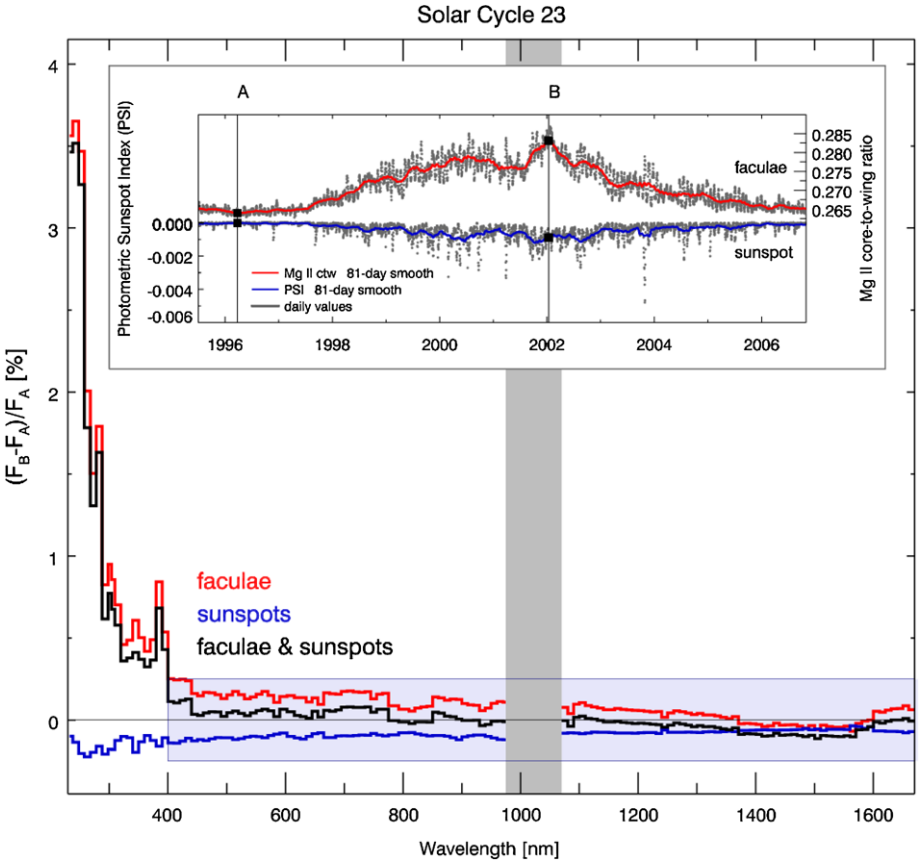

Figure 7 Same as Figure 5, except for Solar Cycle 23.

SBUV on *Nimbus*-7, SBUV-2 on NOAA-9 and NOAA-11, and SUSIM and SOLSTICE on UARS.[3] It has a wavelength range from 120 to 400 nm at a sampling rate of 1 nm covering the period from November 1978 to August 2005.

UV Data from SIP Model or Tobiska et al. Formerly called the Solar2000 (S2K), SIP (Solar Irradiance Platform) is an empirical irradiance model that uses several observed irradiances from a variety of sources, rocket, aircraft, ground, and space-borne platforms.[4] It provides solar spectra from the X-rays through the far infrared and integrated irradiance. This solar model and its subsequent improvements are described in Tobiska *et al.* (2000) and Tobiska and Bouwer (2006). Below, we use the model S2K+VUV2002 version SOLAR2000 Research Grade V2.33. VUV2002 (1 – 420 nm) is based on FUV (far UV) and UV (vacuum UV) irradiances from UARS beginning in 1991 as published in Woods and Rottman (2002) and TIMED/SORCE measurements beginning in 2002 that are modeled using daily F10.7 cm flux as proxy. Above 420 nm, the ASTM E-490 reference spectrum

[3] http://lasp.colorado.edu/lisird/cssi/cssi.html.

[4] http://www.spacewx.com/solar2000.html.

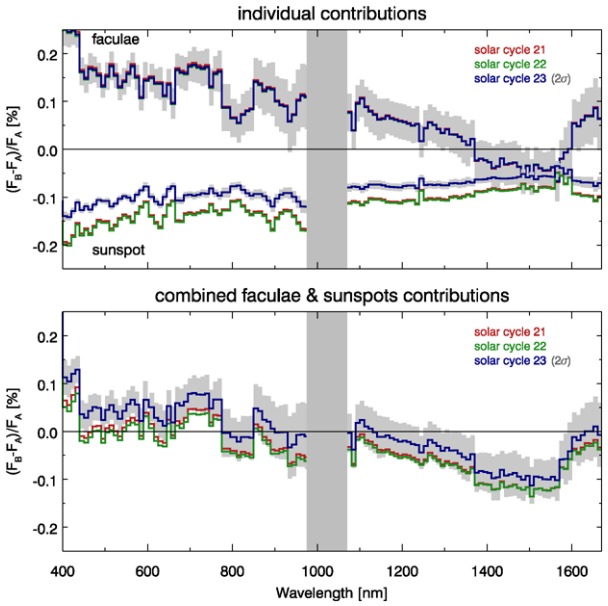

Figure 8 Eleven-year vis-IR variability curves for Solar Cycles 21 – 23 (see also Figures 5 – 7). The gray shaded region represents the 2σ uncertainties from model regression parameters during Solar Cycle 23.

is used, whose integrated total irradiance is scaled to agree with TSI (Fröhlich and Lean, 1998). In the latter spectral region, no solar variability is modeled. For more details, see Tobiska *et al.* (2000) and Tobiska and Bouwer (2006).

UV-vis-IR Data from NRLSSI Model or Lean et al. The UV-vis-IR irradiance data set by Lean *et al.* (1997, 2005), also called NRLSSI (*Naval Research Laboratory SSI*),[5] is a model popularly used for climate and atmosphere research.

In this model, SSI is calculated empirically on a per-wavelength basis by parametrizing observed irradiances in terms of solar proxies of sunspot area and facular brightening. NRLSSI uses the Mg II index only for wavelengths from 30 to 300 nm. The solar proxy model has been adjusted to TIMED/SEE and UARS/SOLSTICE data in the 0 – 120 nm and 120 – 300 nm wavelength ranges, respectively. Above 300 nm, SSI is a composite of SOLSPEC up to 900 nm and the Kurucz spectrum at longer wavelengths. In this region, model results of sunspot and facular contrasts from the Unruh model are used (Lean, 2000). Its SSI is obtained by constraining the total flux from 120 to 100 000 nm to agree with TSI.[6]

UV-vis-IR Data from SATIRE Model or Krivova et al. The model from Krivova *et al.* or SATIRE (Spectral And Total Irradiance REconstructions) calculates solar irradiances based on the assumption that variations are caused directly by magnetic fields at the surface (Solanki and Krivova, 2004). Using magnetic surface observations from MDI (Michelson Doppler Imager) continuum images and ground-based observations, the SSI is formed by superposition of representative model irradiances for quiet sun, sunspot umbrae and penumbrae, and networks (Kurucz, 1993; Unruh, Solanki, and Fligge, 1999; Krivova *et al.*, 2003; Krivova, Solanki, and Floyd, 2006).

[5] http://lasp.colorado.edu/LISIRD/NRLSSI/NRLSSI.html.

[6] For more details, see for example: http://www.geo.fu-berlin.de/en/met/ag/strat/forschung/SOLARIS/Input_data/Calculations_of_Solar_Spectral_Irradiance_Oct07.pdf.

Below 300 nm, a semi-empirical approach (Krivova, Solanki, and Floyd, 2006) is used to extend to shorter wavelengths (down to 115 nm). The approach uses SUSIM/UARS and Mg II ctw ratio to obtain an improved estimate of solar cycle variations between 240 and 400 nm.

In the comparison, we use the SATIRE version[7] as of February 2009 (Krivova *et al.*, 2009; Krivova, Solanki, and Unruh, 2011).

UV-vis-IR Measurements from SIM/SORCE or Harder et al. SIM (Spectral Irradiance Monitor) aboard SORCE (*Solar Radiation and Climate Experiment*) is a dual Fèry prism spectrometer (Harder *et al.*, 2005a, 2005b). SIM measures full-disk UV-vis-IR spectral irradiances in the 300 – 2400 nm range at 0.25 – 33 nm spectral resolution. The SIM solar spectra have an absolute accuracy of 2 – 8% and are daily available since May 2003. The daily spectra we use here are version 17 SIM data.[8]

4. Intercomparison of the SCIA Proxy with Other Solar Data

Figures 9 – 12 show daily SSI timeseries of all solar data that are compared here. The wavelength intervals correspond to the eight panels shown in Figures 3 and 4. Except for SUSIM (1991 – 2005) and SIM (2003 – present), all SSI timeseries cover the entire satellite era (1978 – 2008).

In the UV (Figure 9), SCIA proxy (SATIRE) appears highest (lowest) in both panels. In these intervals, SUSIM appears to be in near agreement with NRLSSI. SIM, on the other hand, is in near agreement with SIP model and DeLand & Cebula composite, which are intermediate between SCIA proxy and NRLSSI. It should be noted that SUSIM forms the DeLand & Cebula UV composite from October 1991 – August 2005, but adjusted to the SBUV data. In the vis-IR region (*cf.* Figures 10 – 12), depending on the wavelength regions, no general statement can be made whether NRLSSI, SATIRE, or SCIA proxy data is highest or lowest with respect to the other data. There is, however, a general similarity between NRLSSI and SATIRE; this is because NRLSSI vis-IR regions use model results of sunspot and facular contrasts from the Unruh model (Lean, 2000) similar to SATIRE. SIM, on the other hand, appears to be the highest in almost all intervals. Except for the UV spectral range, the biases between the data is within 1% well below the absolute accuracy of about 2 – 3% for solar measurements.

Regarding the shape of rise and fall of absolute SSI over the course of the three solar cycles, the UV composite from DeLand & Cebula stands out especially in the years 1986 – 1989 and 1991 – 1993. Referring to Figure 8 of DeLand and Cebula (2008), the UV SSI are derived from the three instruments *Nimbus*-7, NOAA-9, and NOAA-11, and the two instruments NOAA-9 and NOAA-11, during these time periods as shown in the top and bottom panels of Figure 9, respectively. This suggests a discontinuity in overlapping data sets. The main reason for this is that the normalization used for NOAA-9 to merge with the other SBUV data is inaccurate in Figures 10 and 13 of DeLand and Cebula (2008).

Except for parts of the DeLand & Cebula composite, all solar data are in-phase with the 11-year solar cycle. The DeLand & Cebula composite (therefore also SUSIM) is the only set of data that reproduces the sharp double peak of Cycle 23. The other solar data show a

[7] See http://www.mps.mpg.de/projects/sun-climate/data.html.

[8] See http://lasp.colorado.edu/sorce/data/ssi_data.htm.

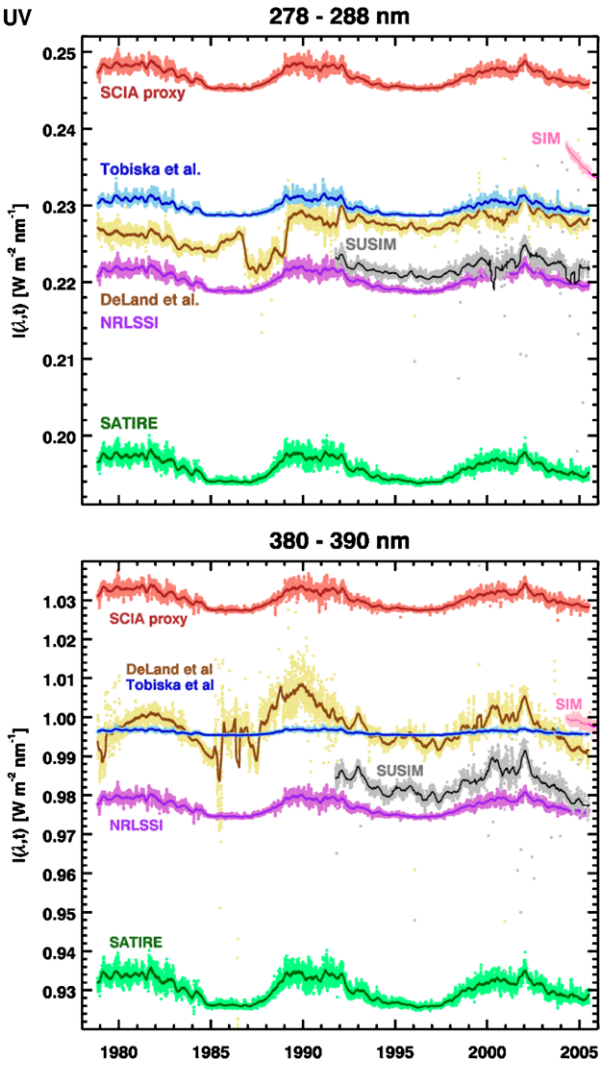

Figure 9 SSI timeseries in the UV. Top and bottom panels show daily absolute UV values in 278 – 288 nm (containing the Mg II doublet), and 380 – 390 nm (containing the Ca II doublet), respectively. Each panel shows daily (dots) and 81-day smoothed (solid line) values. Except for SUSIM and SIM, all timeseries extend from November 1978 to July 2005.

double peak with a smaller maximum peak. With regard to variations from solar minimum to maximum, the SIP/Solar2000 model shows the lowest amplitude especially in the second UV interval at around 385 nm. One should keep in mind that over a solar cycle all satellites show changes in the near UV well below 1%, which is below the long-term stability of any satellite instruments. Nevertheless, good qualitative agreement is seen in the satellite data sets. In the vis-IR regions (Figures 10 – 12), amplitudes of variability appear to get smaller and smaller from short to long wavelength regions for all data shown.

In the vis-IR intervals, only NRLSSI remains in-phase with the solar cycle with possible exception in the 1550 – 1560 nm wavelength interval. This may be attributed to the way the absolute magnitude of the integrated spectra is constrained to agree with the actual bolometric TSI observations (Lean *et al.*, 2005). In the visible region, the sunspot darkening and facular brightening contribution is nearly canceling in the SCIA proxy model, indicating no clear phase relationship with the 11-year solar cycle. The SATIRE model is similar to

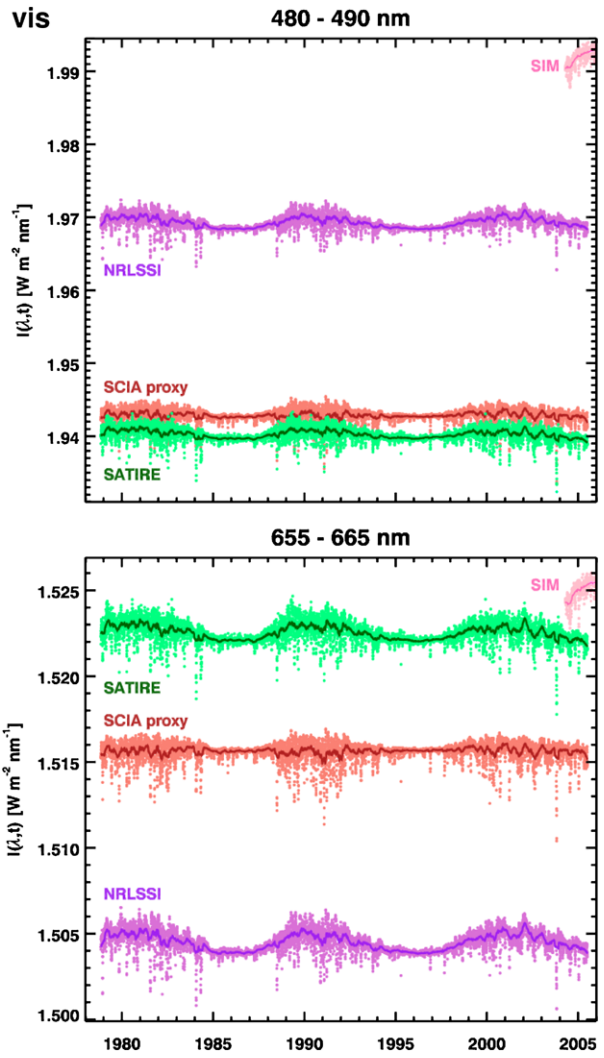

Figure 10 SSI timeseries in the visible range. (Top) 480 – 490 nm and (bottom) 655 – 665 nm containing the Hβ and Hα Balmer absorption lines, respectively.

NRLSSI being in-phase in the visible. In the near-IR, SCIA proxy appears to be out-of-phase in both intervals (Figure 12), while SATIRE appears only out-of-phase at the longer wavelength interval near 1555 nm. As shown in Figure 14 below, these differences in the phasing with solar cycle will result in low correlation coefficients at longer wavelengths between the various data sets.

By considering only the timeseries of solar proxies during the years 1972 – 2008 (*cf.* Figure 1), the last solar cycle is the weakest among the three. This is seen in Figures 3 and 4 and also in Figures 9 – 12. In terms of the contribution of UV variability to TSI variability, Table 3 shows that Solar Cycle 23 has the lowest UV contribution. This is consistent with results, for example, by Willson and Mordvinov (2003), de Toma *et al.* (2004), Wenzler *et al.* (2006), Fröhlich (2009), and Wenzler, Solanki, and Krivova (2009), using other solar activity indicators.

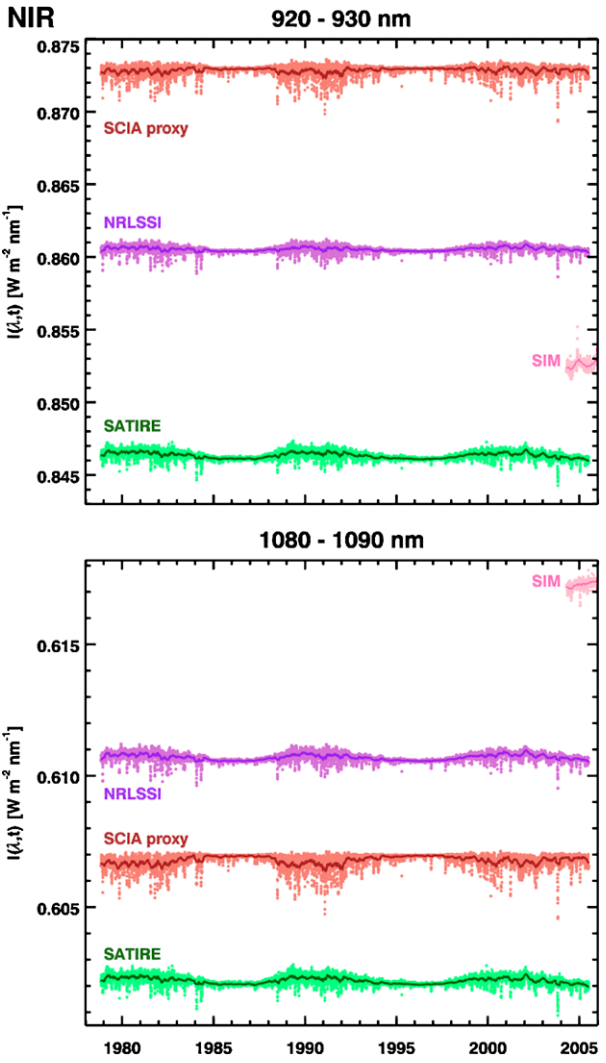

Figure 11 SSI timeseries in the NIR range. (Top) 920 – 930 nm and (bottom) 1080 – 1090 nm containing the He I multiplet.

As SIM covers only the time period 2004 – 2008, only its behavior during the descending phase of Solar Cycle 23 can be characterized. In general, SIM shows a more negative trend in the UV spectral region than all other data, while in the visible region SIM shows an opposite trend. SIM's trend in the vis region (Figure 10) is opposite to the other solar data. SATIRE and SCIA proxy are in agreement with SIM's trend in the SWIR (Figure 12) but in the NIR region only the SCIA proxy agrees (Figure 11).

Figure 13 shows the 22-year (1978 – 2005) solar mean and standard deviation as a function of wavelength for all data sets. The mean (top panel) and standard deviations (bottom panel) are computed using different statistics, namely, ordinary (solid line) and robust (solid dashed dot line) statistics. Ordinary statistics are calculated based on minimizing square of differences. Robust statistics are calculated using mean deviates and adjustable weights to remove outliers. Here, mean deviates with bisquare weighting are used to calculate the robust mean. Two bisector fits *x versus y* and *y versus x* are used to determine the distance to

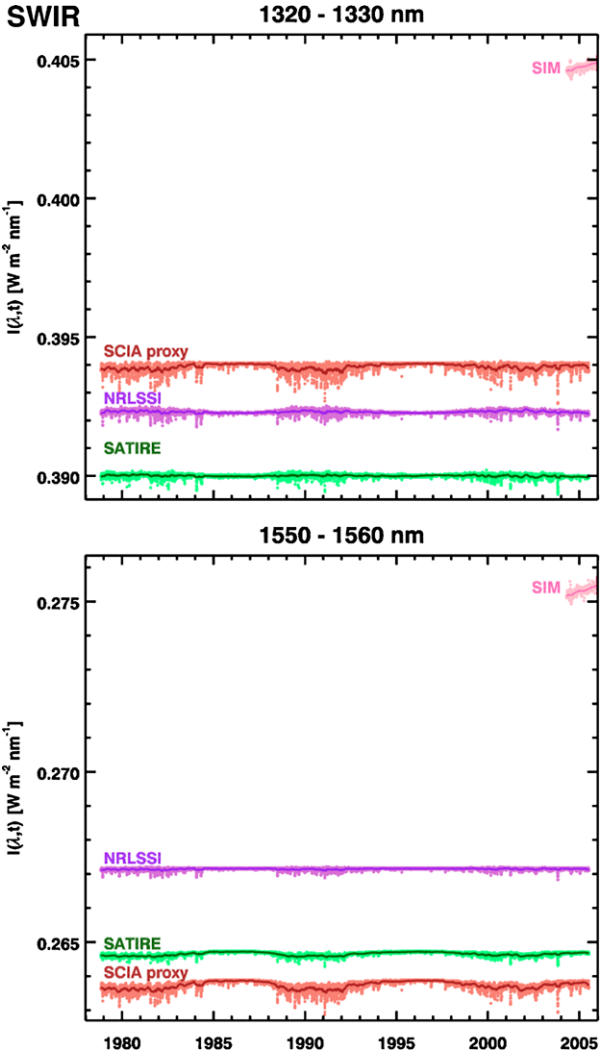

Figure 12 SSI timeseries in the SWIR range. (Top) 1320 – 1330 nm and (bottom) 1550 – 1560 nm near the opacity H^- minimum.

the slope in each dimension under the assumption that there are no independent variables. The weights are then determined using Tukey's biweights (Hoaglin, Mosteller, and Tukey, 1983). Outliers receive less weights than points close to the respective slopes, or zero weight. Using these new weights mean deviates, standard deviation, and correlation are determined.

There are no noticeable differences between the solar mean irradiances (*cf.* top panel of Figure 13) except for some very small deviations at certain wavelength intervals such as the 300 – 500 nm region, and a few wavelengths in the IR. For example, the DeLand & Cebula composite is highest in 320 – 400 nm. The DeLand & Cebula composite has been normalized to the Thuillier *et al.* (2004) reference spectrum, which determines their absolute scale. SATIRE is lowest about 330 – 520 nm. SCIA proxy is highest from 670 – 1100 nm, where NRLSSI and SATIRE agree well for most part. The good agreement in the visible and near-IR between SATIRE and NRLSSI comes from the fact that for this wavelength region similar representative solar spectra are used in the modeling. The absolute scale of

the SATIRE and NRLSSI depend on their normalization (filling factor) for a best match to TSI timeseries (Krivova *et al.*, 2009; Krivova, Solanki, and Unruh, 2011). Overall, there are significant deviations (10 – 20%) among the solar data in the UV, while good agreement (less than 5%) in the vis-IR regions exists.

In the bottom panel of Figure 13, large differences in the standard deviation about the mean occur at about 250 – 420 nm and in the IR at about 850 – 1680 nm. NRLSSI, SATIRE, and SCIA proxy seem to be in good agreement from 450 to 850 nm. In the UV, among the SSI data considered, the SIP model shows the lowest variations with solar cycle. In contrast, the DeLand & Cebula composite and SUSIM are the highest among the SSI data. SUSIM is maximum at about 250 – 310 nm and the DeLand & Cebula composite at 320 – 380 nm. In the vis-IR, there is an overall agreement between SATIRE and SCIA proxy across the wavelength range except at 900 nm, where SCIA proxy is maximum.

Standard deviations of each data set as shown in the bottom panel of Figure 13 are computed using ordinary statistics (least squares, solid line) and robust statistics (least absolute deviation, solid dashed-dot line). The larger the deviations between the two standard deviations are, the more contaminations from outliers.

Figure 14 shows correlation coefficients as a function of wavelength. Correlations are as high as 0.75 in the vis-NIR regions, while it ranges from 0.25 – 0.95 in the UV and 0.12 – 0.60 in the SWIR. In general, due to the disagreements in the phasing with solar cycles, there is an overall decrease of correlation toward long wavelengths.

Each data set show significant differences in robust and ordinary standard deviations in different wavelength regions. For example, in the UV, largest deviations are seen in the DeLand & Cebula composite while other solar data show no deviations. The larger differences seen in the DeLand & Cebula composite are due to additional errors that come from the merging procedure of the various irradiance data sets. All other data sets rely more on proxy data that are generally more precise. In the vis-IR, deviations reach maximum at different wavelengths, *e.g.*, SCIA proxy at about 1150 nm, SATIRE at about 1350 nm, and NRLSSI at about 1550 nm. The SCIA proxy shows a factor of two to four larger deviations than SATIRE and NRLSSI in the NIR.

Figure 15 shows a scatterplot corresponding to the timeseries in the 1550 – 1560 nm interval shown in Figure 12, which is representative of SSI variability in SWIR range. Shown in this figure are scatter plots that are grouped vertically from left to right with respect to SCIA proxy, SATIRE, and NRLSSI, respectively. From this scatterplot, we calculate, using ordinary and robust statistics as summarized in Table 2, mean, standard deviation about the mean, and correlation. While the means in the 1550 to 1560 nm spectral range do not differ largely, the standard deviations are quite different. The standard deviations over two solar cycles (1978 – 2005) are doubled for SATIRE and four times larger for the SCIA proxy as compared to NRLSSI. Differences appear when ordinary and robust statistics are used to calculate standard deviations and correlations between data sets. When the x and y values are interchanged in the statistical analysis, we found no significant differences when using ordinary statistics or robust statistics, except between NRLSSI and SATIRE in the robust case. This can be particularly seen in the angle change from unity slope (45 degree) in the scatter plot, which changes significantly when interchanging axes for NRLSSI and SATIRE (see Table 2).

4.1. Eleven-Year Timescales

So far we compared SSI variability on daily timescales. Now we quantify how the SCIA proxy changes from solar minimum to solar maximum in the 11-year solar cycle timescales

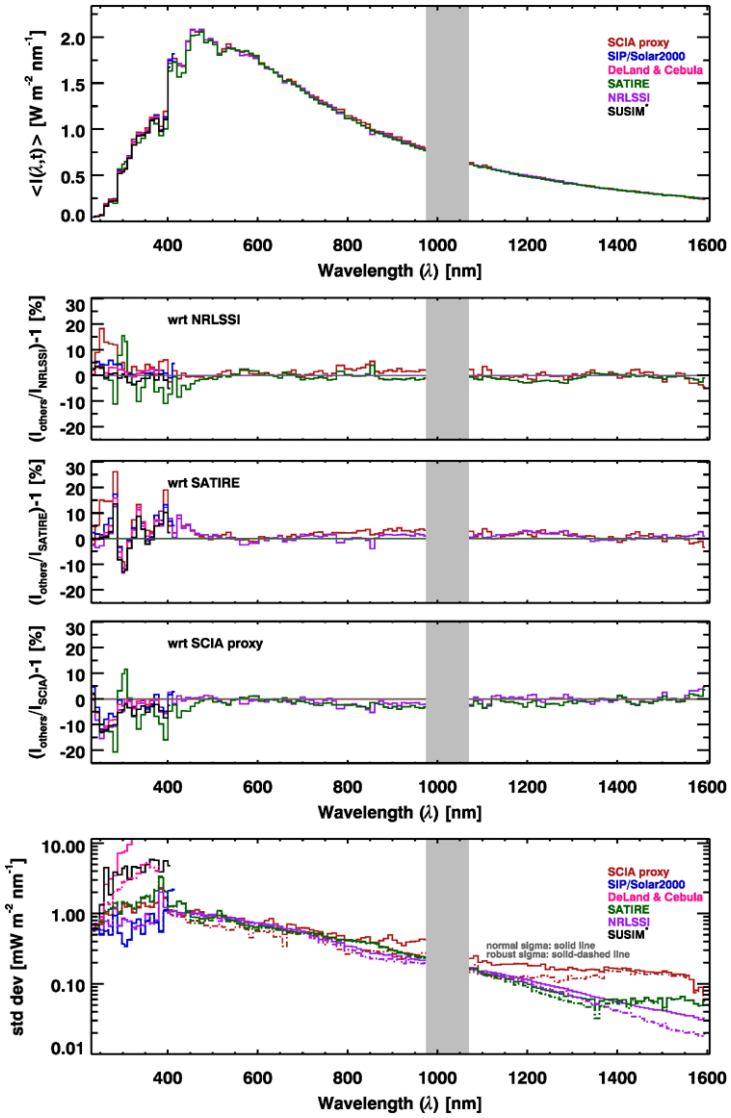

Figure 13 From top to bottom: mean SSI, percent difference with respect to NRLSSI, SATIRE, and SCIA proxy; and standard deviation about the mean. Except for SUSIM, which covers only the years 1991 – 2005 (at common 4441 days), the quantities are calculated from the entire satellite era (1978 – 2005), at common 9759 days to all SSI data. Standard deviations using ordinary in least squares sense (solid line) and robust in least absolute deviate sense (dot-dashed line) are shown in the bottom panel.

with respect to the other SSI data. We determine the percent change (Equation (4) for Solar Cycles 21 – 23). These are shown in Figures 16 and 17. Solar minima and solar maxima are defined by extrema in the 81-day smoothed Mg II index (top panel of Figure 1). The irradiances or solar proxies are then averaged over 81 days about the solar maximum and minimum dates.

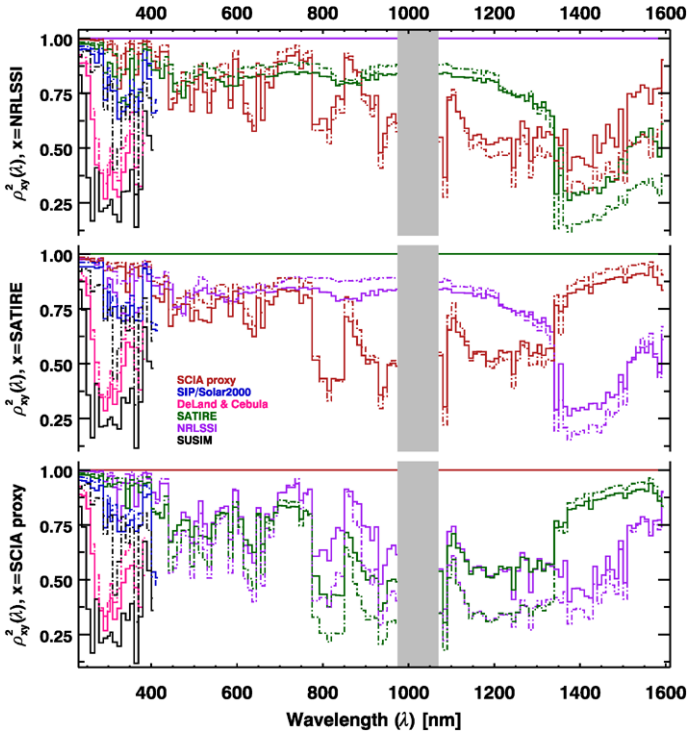

Figure 14 Correlation coefficients as a function of wavelength. In both ordinary (solid) and robust (dashed) definitions, we show ρ^2_{xy} as a function of wavelength with respect to NRLSSI (top), SATIRE (middle), and the SCIA proxy (bottom).

Different estimates of the Sun's UV irradiance to TSI exist in the literature and are briefly reviewed in Krivova, Solanki, and Floyd (2006). From Figure 16, we can derive the percent variation of TSI that is due to UV. In particular, we integrate SSI to obtain ΔF_λ over the wavelength intervals, 250 – 300 nm, and 300 – 400 nm. Using 81-day average TSI values from PMOD/WRC[9] at the same solar cycle extrema dates as used for the SSI data, the changes of TSI during the 11-year solar cycle, $\Delta F_{\rm tot}$, can be calculated during Cycles 21 – 23, which are 0.949 W m^{-2}, 0.838 W m^{-2}, and 1.382 W m^{-2}, respectively. The percent UV variation is summarized in Table 3. Among these intervals, the 300 – 400 nm interval contributes the most (*i.e.*, more than 50%) to the solar cycle change of TSI. This is observed only by SATIRE[10] in Solar Cycles 21 and 22, and by the DeLand & Cebula composite and SUSIM in Solar Cycle 23. It should be noted that SUSIM has a long-term uncertainty that is comparable or exceeds SSI variability between solar maximum and minimum (Krivova, Solanki, and Floyd, 2006). Other solar data give less than 40% TSI contribution in the near UV. The normalization problem in the NOAA-9 data leads to larger near UV irradiance change in Solar Cycle 22 compared to other data.

[9] See ftp://ftp.pmodwrc.ch/pub/data/irradiance/composite/DataPlots/ext_composite_d41_62_1007.dat.

[10] Krivova, Solanki, and Floyd (2006) used different solar extrema dates Oct – Nov 1996 and Apr – May 2000, *i.e.*, different levels of solar activity, which may contribute to different estimates of percent variation of TSI that is due to UV.

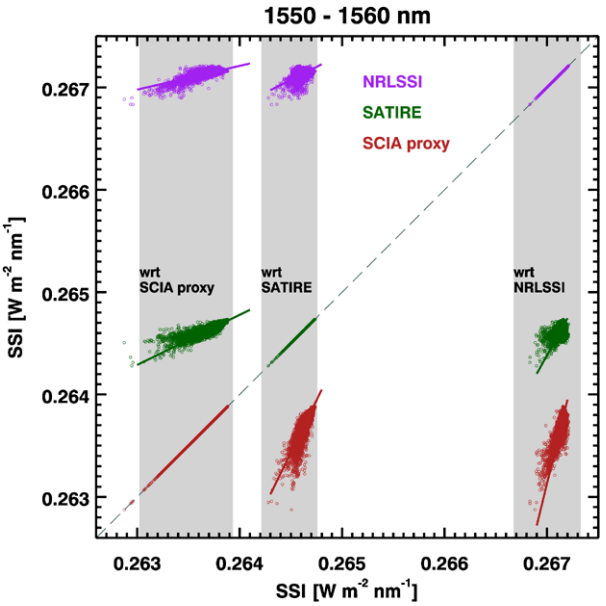

Figure 15 Scatter plots of SSI timeseries in the SWIR range. Grouped vertically from left to right are scatter plots with respect to SCIA proxy, SATIRE, and NRLSSI, respectively.

In the UV, the SIP model (or Solar2000) appears to show the lowest variability in Cycles 22 and 23. NRLSSI's variability is slightly higher than SIP. SATIRE and SCIA proxy agree well with each other except at 300 – 400 nm, where SATIRE is higher than SCIA proxy. In the vis-IR, NRLSSI and SATIRE agree with each other. The SCIA proxy is here lower than the two other data, oscillates around zero from 450 – 750 nm and dips to negative values above 750 nm. The dip in the SCIA proxy at 750 – 850 nm is probably due to the aluminum surface on mirrors in SCIAMACHY (Pagaran, Weber, and Burrows, 2009). The other dip is observed in the 1370 – 1570 nm interval near the H^- opacity minimum, where both sunspots and so-called dark faculae contribute to lower irradiances at solar maximum (Solanki and Unruh, 1998; Unruh *et al.*, 2008). Both SATIRE and the SCIA proxy reproduce this dip, but NRLSSI does not. Above 1570 nm, only SCIA proxy shows an increase from -0.14% to near zero values. This rise is not evident in NRLSSI and SATIRE.

Harder *et al.* (2009) reported on irradiance changes in selected spectral regions during the descending phase (April 2004 to November 2007) of Solar Cycle 23. Bottom subpanel of Figure 18 shows the irradiance changes using ten-day average from 21 April to 01 May 2004 ($\langle P_a(t)\rangle \simeq 0.2688$) and 05 to 14 November 2007 ($\langle P_a(t)\rangle \sim 0.2636$). The four spectral regions shown are 240 – 400 nm, 400 – 691 nm, 691 – 972 nm, and 972 – 1600 nm, representing the UV, vis, NIR, and SWIR regions, respectively. Since the SCIA proxy has a data gap at 950 – 1070 nm (*cf.* Figure 1), the NRLSSI or SATIRE model was scaled to the SCIA proxy near the two boundaries of the gap and then added to fill this gap. Similarly the irradiance change during the descending phase for Cycles 21 and 22 can be determined for the other solar data sets used in this study, *cf.* top and center subpanels of Figure 18, respectively. The periods for Solar Cycles 21 and 22 are chosen such that Mg II index changes are similar to Solar Cycle 23, as shown in Figure 18.[11]

[11]This period is between 25 October to 03 November 1983 and 01 to 10 July 1986 for Solar Cycle 21 and between 28 January to 06 February 1994 and 14 to 23 August 1996 for Solar Cycle 22.

Table 2 Ordinary and robust statistics of SWIR SSI timeseries. The quantities below are computed from the bottom panel of Figures 12 (excluding SIM) and 15.

Quantity	Mean $\times 1$ W nm^{-1} m^{-2}		Std. dev. $\times 10^{-5}$ W nm^{-1} m^{-2}	
SWIR timeseries	Ordinary	Robust	Ordinary	Robust
NRLSSI	0.267	0.267	3.55	2.09
SATIRE	0.265	0.265	5.84	5.82
SCIA proxy	0.264	0.264	13.1	12.3

Quantity	Correlation					
SWIR timeseries	Ordinary			Robust		
$x \backslash y$	NRLSSI	SATIRE	SCIA proxy	NRLSSI	SATIRE	SCIA proxy
NRLSSI	1.00	0.55	0.77	1.00	0.33	0.55
SATIRE	0.55	1.00	0.90	0.58	1.00	0.95
SCIA proxy	0.77	0.90	1.00	0.76	0.94	1.00

Quantity	Angle with respect to unity slope [degrees]					
SWIR timeseries	Ordinary			Robust		
$x \backslash y$	NRLSSI	SATIRE	SCIA proxy	NRLSSI	SATIRE	SCIA proxy
NRLSSI	45.00	2.85	25.71	45.00	16.02	31.29
SATIRE	26.47	45.00	18.75	18.21	45.00	18.91
SCIA proxy	33.14	23.09	45.00	31.96	18.96	45.00

During the descending phase of Solar Cycle 23, SIM shows more than four times larger changes in the UV compared to the models (SCIA proxy, SATIRE, and NRLSSI), which is similar to what we found in Figures 9 – 12 on daily timescales. SATIRE and NRLSSI have comparable ΔF_λ values in the vis-IR and are (about three times) larger than the SCIA proxy. SIM shows in the vis an opposite trend with respect to SCIA proxy, SATIRE, and NRLSSI. Also the absolute magnitude of the change in the visible is about more than twice larger than for the other data. In the SWIR, NRLSSI and SATIRE, which are both positive, the changes are comparable in magnitude. The SCIA proxy and SIM are negative in this region. Among the three models, only SCIA proxy reproduce the negative sign or out-of-phase signature in SWIR in agreement with SIM. In Solar Cycle 22, the DeLand & Cebula composite and SUSIM measurements show ΔF_λ in the UV by a factor of 2 – 3 larger compared to the models. They are almost half that of SIM in Cycle 23. In the vis-IR, all models show a non-negative ΔF_λ in both Cycles 21 and 22.

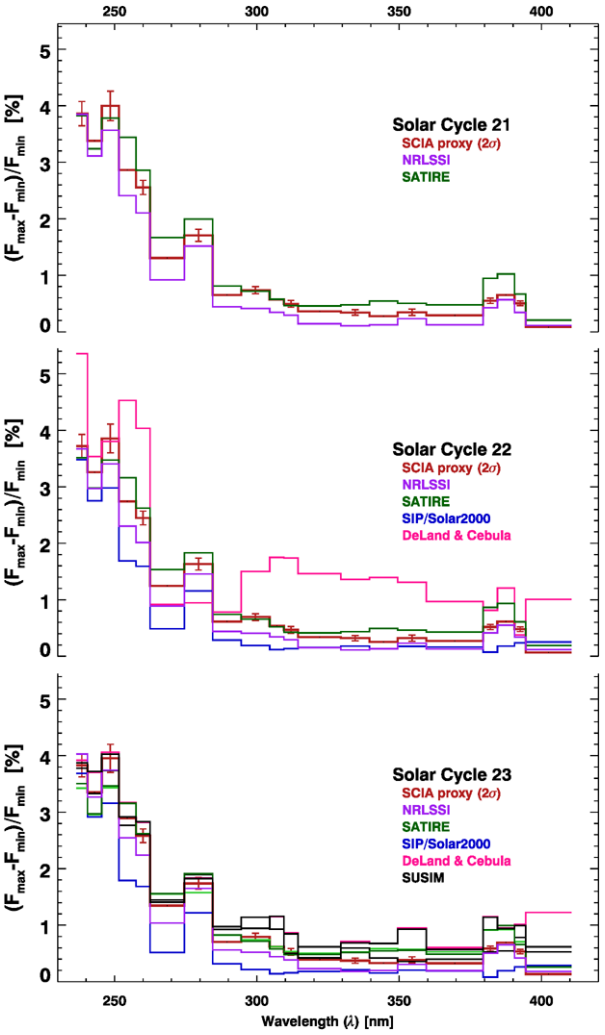

Figure 16 Comparison of eleven-year percent UV changes between solar maximum and solar minimum of Solar Cycles 21 (top), 22 (middle), and 23 (bottom), respectively. 2σ uncertainty is only shown for the SCIA proxy model.

Table 4 shows SSI total flux changes over the range 240 – 1600 nm and changes from various TSI data during Solar Cycle 23. From this table, we can see that NRLSSI ($+0.432$ W m^{-2}) is constrained to agree with TSI from TIM/SORCE ($+0.495$ W m^{-2}) (Lean *et al.*, 2005). Similarly, SATIRE, whose free parameter $B_{\rm sat}$ value is derived from a VIRGO TSI timeseries fit, has a numerical value ($+0.578$ W m^{-2}) almost equal to TSI from VIRGO/SOHO. The SIM degradation corrections included a correction to match the SIM integrated SSI trends to the TIM TSI long-term trend (Harder *et al.*, 2009). For the spectral region 240 – 1600 nm the integrated SSI change is a bit smaller than TIM TSI change, similar to the other models which have lower changes than seen in the corresponding TSI used to constrain them. The SCIA proxy, which was not constrained to the TSI shows much smaller changes in the 240 – 1600 nm spectral interval during the descending phase of Solar Cycle 23.

Figure 18 and Table 4 may be considered as an expanded view of Figure 3 in Harder *et al.* (2009), including different data sets and including comparisons to Solar Cycles 21 and 22.

Table 3 Percent UV variation of Solar Cycles 21 – 23. Column (1) lists the solar data used in this study, cols. (2) – (5) the wavelength intervals 250 – 300 nm, and cols. (6) – (7) 300 – 400 nm; in each column the UV changes ΔF_λ with respect to solar cycle changes in TSI, $\Delta F_{\rm tot}$, between solar maximum and minimum of Solar Cycles 21 – 23 are indicated. We use $\Delta F_{\rm tot}$ from PMOD/WRC TSI that starts from 1976 to present. Using the same dates of extrema used in solar proxies (see Figure 2), the TSI changes, $\Delta F_{\rm tot}$, during cycles 21 – 23 are 0.949 W m^{-2}, 0.838 W m^{-2}, and 1.382 W m^{-2}, respectively.

λ interval:	250 – 300 nm [%]			300 – 400 nm [%]		
Solar Cycle	21	22	23	21	22	23
SCIA proxy	15.4	16.6	11.0	39.4	41.8	29.8
NRLSSI	11.5	12.7	9.0	23.0	26.1	21.1
SATIRE	17.8	18.5	11.8	54.5	56.2	38.5
SIP/Solar2000		9.1	5.9		18.3	12.8
DeLand & Cebula		20.2	12.9		132.4	55.9
SUSIM			12.5			52.2

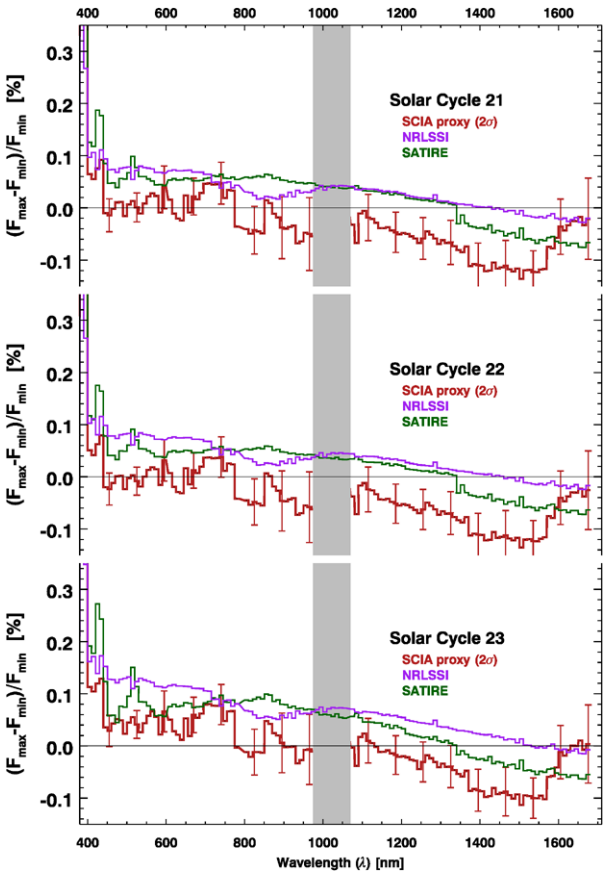

Figure 17 Same as Figure 16, except for the vis-IR spectral regions (390 – 1680 nm).

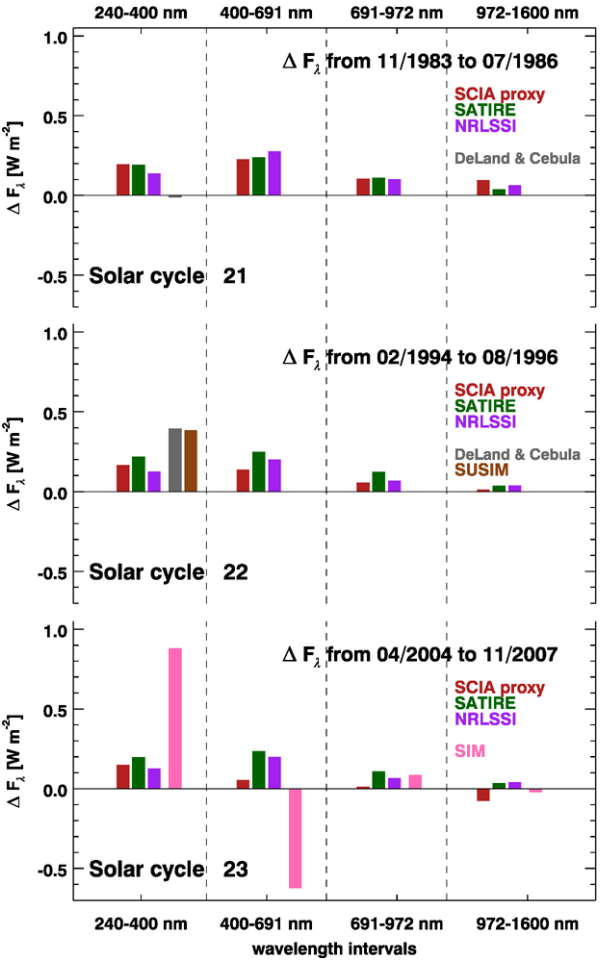

Figure 18 Top to bottom panels show the change of SSI during the descending phase of Solar Cycles 21 – 23, respectively. The bar chart compares the irradiance change from near solar minimum to near solar maximum at selected dates during the descending phase of each solar cycle. The dates are chosen in such a way that the differences between the ten-day averaged Mg II index values are about the same in each solar cycle.

5. Discussion

The majority of the solar data considered here are based upon empirical models or a proxy model where solar proxies were scaled to observations in a limited time period. These models are in certain ways similar, since they assume irradiance variability to originate from competing bright faculae and dark sunspots related to magnetic surface activity on the Sun. SATIRE and the SCIA proxy include both faculae and sunspot components for the entire wavelength region from UV to near-IR. The SIP and UV portion of NRLSSI use only the faculae term F10.7 cm flux, or the Mg II ctw ratio, to describe the SSI variation. Their low amplitudes of absolute and relative UV variability, as we have found, may be due to the use of a single proxy in modeling irradiances. Only results from SUSIM/UARS and SIM/SORCE SSI are derived from direct measurements and from a single instrument. The DeLand & Cebula composite is also derived from direct measurements but from several instruments and platforms. The merging approach in the DeLand & Cebula composite makes this long-term data set independent of any proxy data and index. This data set may not be perfectly homogenized, but it can be intercalibrated using the F10.7 cm flux (Lockwood *et al.*, 2010).

Table 4 Changes in integrated SSI between 240 and 1600 nm and TSI from November 2007 (near solar minimum) to April 2004 (two years after solar maximum of Solar Cycle 23).

SSI data	ΔF_λ [W m^{-2}]
NRLSSI	+0.432
SATIRE	+0.578
SCIA proxy	+0.147
SIM/SORCE	+0.322
TSI data	**ΔF [W m^{-2}]**
PMOD/WRC vd41.61	+0.588
VIRGO/SOHO v6	+0.576
TIM/SORCE v12	+0.519

Dudok de Wit *et al.* (2009a) have shown by using their multiscale approach that a single proxy modeling is not sufficient to properly model UV irradiances. Regarding the use of F10.7 cm flux in the SIP model and the Mg II index in NRLSSI, we have found that the latter gave higher amplitudes of UV variability than the former, confirming that the Mg II index is a more suitable facular brightening proxy than F10.7 cm flux (Viereck *et al.*, 2001). Similar to the SIP and NRLSSI models, the SCIA proxy is based on solar proxies. It uses the Mg II index for facular brightening and PSI for sunspot darkening. By contrast, SATIRE has more than two components, which also include sunspot umbrae and penumbrae and the bright network. While the latter model (SATIRE) calculates its irradiances from a solar atmosphere model, the former models (SCIA proxy, NRLSSI, SIP) rely on transforming a change of proxies to changes of irradiance as a function of wavelength, assuming linearity. This assumption is challenged by the results from the short timeseries from SIM. In general, Figure 18 suggests that proxy-based models and SATIRE not only gave smaller magnitude of variability across the UV-vis-IR spectral regions than SIM but also gave a different sign (or phase) of variability especially in the vis-IR regions (Garcia, 2010; Gray *et al.*, 2010; Haigh *et al.*, 2010).

SATIRE (Unruh, Solanki, and Fligge, 1999; Fligge, Solanki, and Unruh, 2000) derives its basic intensities from a more physics-based solar atmosphere model (Kurucz ATLAS9 (Kurucz, 1993)). The rest of the models (SIP, NRLSSI, and SCIA proxy) rely on direct irradiance observations, *i.e.*, SOLSTICE aboard UARS in SIP and NRLSSI, and SCIAMACHY in SCIA proxy. While SIP and NRLSSI use the same UV data (SOLSTICE/UARS) to model irradiances, the differences between them may be mainly coming from the use of different faculae proxies (F10.7 cm in SIP and Mg II in NRLSSI). Differences between the proxy models may also come from the different time periods that were used to derive the scaling factors for the solar proxies. For instance, the scaling in the SCIA proxy model was derived during the two year period 2003 – 2004, which included the record sunspot darkening during the Halloween storm (October 2003). This may explain the larger dark faculae contribution in the SCIA proxy model as compared to NRLSSI. SATIRE derives the SSI variability from continuum images and magnetograms via the filling-factor approach, the rest of the models from proxies.

Among the SSI data considered that cover the UV-vis-IR spectral range, only the SCIA proxy model is not constrained to agree with the measured TSI. The total solar flux of SATIRE and NRLSSI in the 240 – 1600 nm spectral range is close to the TSI from TIM/SORCE and VIRGO/SOHO, respectively, which were used to constrain the models. While NRLSSI constrains its total flux from 120 to 100 000 nm to the bolometric TSI,

which is a direct TSI constraint; SATIRE, on the other hand, derives its saturation magnetic field strength B_{sat} from a fit to VIRGO TSI timeseries; an indirect TSI constraint. Whether TSI provides a useful constraint for SSI recalibration remains debatable. Without TSI constraints, the SCIA proxy model shows smaller total flux changes in the 240 to 1600 nm spectral range than the other data during Solar Cycle 23.

6. Summary and Conclusions

The SCIA proxy model derives the faculae and sunspot contribution by fitting solar proxies to two years of SCIAMACHY solar data. The solar proxies are then used to extrapolate linearly SSI variations on 11-year solar cycle timescales. In this paper, we applied the SCIA proxy model to reconstruct daily UV-vis-IR SSI (Figures 3 – 4) in the 240 – 1600 nm (with a gap in 975 – 1070 nm) from November 1972 to January 2008. Changes of SSI between solar minimum and solar maximum of Solar Cycles 21 – 23 have been investigated (Figures 5 – 8).

We compared the SCIA proxy SSI variability on daily (Figures 9 – 12) and 11-year timescales (Figures 16 – 17) with UV data from SUSIM, and the DeLand & Cebula composite (SSAI), and model data from SIP/Solar2000, NRLSSI, and SATIRE. About 10 – 20% differences in the multi-annual mean (1978 – 2005) between the data sets are found in the UV, and good agreement, *i.e.*, less than 5%, in the vis-IR (*cf.* second to fourth panels from top of Figure 13). Differences in standard deviations over the entire period 1978 – 2005 are about $+1$ mW m^{-2} nm^{-1} and $+0.05$ to $+0.5$ mW m^{-2} nm^{-1} in the UV and IR, respectively. Correlations between the data sets are as high as $+0.75$ in the vis-NIR regions, while they range from 0.25 – 0.95 in the UV and 0.12 – 0.6 in the SWIR. The SCIA proxy has a moderate correlation of $+0.5$ from 750 to 1350 nm.

Except for the DeLand & Cebula composite in Solar Cycle 22, percent differences in the UV between solar maximum and solar minimum (*cf.* Table 3) are in close agreement for Solar Cycles 21 – 23 for all data. The DeLand & Cebula composite consisting of different SBUVs data show some inhomogeneity (jumps) that resulted in larger differences for Solar Cycle 22 (see Figure 9). The SIP/Solar2000 and NRLSSI cases may be due to the use of a single proxy in the UV irradiance modeling. The SCIA proxy shows intermediate variability in the UV. In the vis-IR, NRLSSI and SATIRE solar cycle variabilities agree with each other, while SCIA proxy shows the lowest variations across the vis-IR range; the latter may be due to overestimation of the sunspot darkening component. Only the SATIRE and SCIA proxy reproduce the negative dip near the H^- opacity minimum (~ 1555 nm), while NRLSSI does not. All models (NRLSSI, SATIRE, and SCIA proxy) show that Solar Cycle 23 is the weakest among the last three solar cycles. During the descending phase of Solar Cycle 23 (*cf.* Figure 18), measurements from SIM show changes in SSI larger in magnitude (UV and vis) and opposite trends in the vis-IR spectral regions compared to the models. In the SWIR, SIM and SCIA proxy changes are out-of-phase with the solar cycle in contrast to NRLSSI and SATIRE, but the magnitudes of the changes are smaller for the SCIA proxy than for SIM. During the same period (*cf.* Table 4), the change of total flux (240 – 1600 nm) is smaller for the SCIA proxy model than for the other data, which were constrained to agree better with TSI.

The knowledge of spectral irradiance over several decades and even over a longer period back in time with temporal resolution from days to decades is important in assessing the role of the magnetically active Sun played in climate variability and change. Our effort in evaluating the wavelength dependence of irradiance variability over several decades, especially in the long wavelength regions (above 300 nm), is a starting point in reconstructing irradiance

backwards in time (if not realistic but at least representative). Using recent measurements and linear extrapolation using solar proxies remains one of the indispensable and straightforwardly used tools in reconstructing spectral irradiance. However, if SIM's magnitude and trend in SSI variability during its current operation are not to be taken provisional (Garcia, 2010; Gray *et al.*, 2010), then we need to find an alternate route to modeling UV-vis-IR spectral irradiances. What remains certain is that despite the limitation from the difficulty in absolute solar spectroscopy the direct irradiance variability measurements, now available above 400 nm, will form a valuable basis for the reconstruction of past and future spectral irradiance.

Acknowledgements SCIAMACHY is a collaboration between Germany, The Netherlands, and Belgium. We are indebted to the entire SCIAMACHY team, whose efforts made this analysis possible. We furthermore thank the European Space Agency (ESA) and DLR for processing SCIAMACHY data. The first two and fourth authors (J.P., M.W., & L.F.) of this paper were part of the International Space Studies Institute (ISSI) team[12] on spectral solar irradiance, whose meetings and discussions have benefited this study. Moreover, J.P. acknowledges the warm hospitality he received during his short but productive visits at Laboratory for Atmospheric and Space Physics (LASP) and Max Planck Institute for Solar System Research (MPI-SSR) during the summers of 2008 and 2009, respectively.

We thank Laura Balmaceda of MPI-SSR (now at University of Valencia, Spain) for the homogenized composite PSI sunspot darkening proxy, W. Kent Tobiska of Space Environment Technologies (spacewx.com) for SIP/SOLAR2000 Research Grade V2.33, Judith Lean of Naval Research Laboratory for NRLSSI data, and Jerald Harder of LASP for SIM/SORCE version 17 SSI data. We are grateful to Natalie Krivova of MPI-SSR for providing SATIRE data and in-depth discussions/comments on the manuscript.

This work has been supported by the Deutsche Forschungsgemeinschaft (DFG) project SOLOZON[13] (DFG WE 3647/1-1) within the CAWSES (Climate and Weather Sun–Earth System) national priority programme. Permission to use unpublished data from the VIRGO Experiment on the cooperative ESA/NASA Mission SOHO, TSI data from PMOD/WRC, Davos, Switzerland; TSI data from TIM/SORCE, LASP, Boulder, Colorado is acknowledged.

References

Arnold, N.: 2002, Solar variability, coupling between atmospheric layers and climate change. *Proc. Roy. Soc. London A* **360**, 2787 – 2804. doi:10.1098/rsta.2002.1091.

Balmaceda, L.A., Solanki, S.K., Krivova, N.A., Foster, S.: 2009, A homogeneous sunspot areas database covering more than 130 years. *J. Geophys. Res.* **114**, A7104. doi:10.1029/2009JA014299.

Beasley, A.J., Cram, L.E.: 1990, Stellar analogues of the solar cycle and activity. *Solar Phys.* **125**, 191 – 207. doi:10.1007/BF00154789.

Bonnet, R.M.: 1981, The role of space techniques in the understanding of solar variability. *Solar Phys.* **74**, 485 – 501. doi:10.1007/BF00154532.

Bovensmann, H., Burrows, J.P., Buchwitz, M., Frerick, J., Noël, S., Rozanov, V.V., Chance, K.V., Goede, A.P.H.: 1999, SCIAMACHY: mission, objectives, and measurement modes. *J. Atmos. Sci.* **56**, 127 – 150.

Brueckner, G.E., Edlow, K.L., Floyd, L.E., Lean, J.L., Vanhoosier, M.E.: 1993, The Solar Ultraviolet Spectral Irradiance Monitor (SUSIM) experiment on board the Upper Atmosphere Research Satellite (UARS). *J. Geophys. Res.* **98**(D6), 10695 – 10711. doi:10.1029/93JD00410.

Brueckner, G.E., Floyd, L.E., Lund, P.A., Prinz, D.K., Vanhoosier, M.E.: 1995, Solar ultraviolet spectral-irradiance observations from the SUSIM-UARS experiment. *Metrologia* **32**, 661 – 665. doi:10.1088/0026-1394/32/6/53.

Burrows, J.P., Weber, M., Buchwitz, M., Rozanov, V., Ladstätter-Weißenmayer, A., Richter, A., Debeek, R., Hoogen, R., Bramstedt, K., Eichmann, K.U., Eisinger, M., Perner, D.: 1999, The Global Ozone Monitoring Experiment (GOME): Mission concept and first scientific results. *J. Atmos. Sci.* **56**, 151 – 175.

[12] http://www.issibern.ch/teams/solarspect/.

[13] http://www.iap-kborn.de/CAWSES-Projekt-SOLOZON.373.0.html.

de Toma, G., White, O.R., Chapman, G.A., Walton, S.R., Preminger, D.G., Cookson, A.M.: 2004, Solar Cycle 23: An anomalous cycle? *Astrophys. J.* **609**, 1140 – 1152. doi:10.1086/421104.

de Wit, T.D., Watermann, J.: 2010, Solar forcing of the terrestrial atmosphere. *C. R. Geosci.* **342**(4 – 5), 259 – 272. doi:10.1016/j.crte.2009.06.001.

DeLand, M.T., Cebula, R.P.: 1993, Composite Mg II solar activity index for Solar Cycles 21 and 22. *J. Geophys. Res.* **98**, 12809 – 12823.

DeLand, M.T., Cebula, R.P.: 2008, Creation of a composite solar ultraviolet irradiance data set. *J. Geophys. Res.* **113**, A11103. doi:10.1029/2008JA013401.

Domingo, V., Ermolli, I., Fox, P., Fröhlich, C., Haberreiter, M., Krivova, N., Kopp, G., Schmutz, W., Solanki, S.K., Spruit, H.C., Unruh, Y., Vögler, A.: 2009, Solar surface magnetism and irradiance on time scales from days to the 11-year cycle. *Space Sci. Rev.* **145**, 337 – 380. doi:10.1007/s11214-009-9562-1.

Dudok de Wit, T., Kretzschmar, M., Lilensten, J., Woods, T.: 2009a, Finding the best proxies for the solar UV irradiance. *Geophys. Res. Lett.* **36**, L10107. doi:10.1029/2009GL037825.

Fligge, M., Solanki, S.K., Unruh, Y.C.: 2000, Modelling irradiance variations from the surface distribution of the solar magnetic field. *Astron. Astrophys.* **353**, 380 – 388.

Floyd, L.E., Cook, J.W., Herring, L.C., Crane, P.C.: 2003, SUSIM's 11-year observational record of the solar UV irradiance. *Adv. Space Res.* **31**, 2111 – 2120. doi:10.1016/S0273-1177(03)00148-0.

Floyd, L., Newmark, J., Cook, J., Herring, L., McMullin, D.: 2005, Solar EUV and UV spectral irradiances and solar indices. *J. Atmos. Solar-Terr. Phys.* **67**, 3 – 15. doi:10.1016/j.jastp.2004.07.013.

Fröhlich, C.: 2009, Evidence of a long-term trend in total solar irradiance. *Astron. Astrophys.* **501**, L27 – L30. doi:10.1051/0004-6361/200912318.

Fröhlich, C., Lean, J.: 1998, Total solar irradiance variations: The construction of a composite and its comparison with models. In: Deubner, F.-L., Christensen-Dalsgaard, J., Kurtz, D. (eds.) *New Eyes to See Inside the Sun and Stars*, *IAU Symp.* **185**, Kluwer Academic, Dordrecht, 89 – 102.

Fröhlich, C., Lean, J.: 2004, Solar radiative output and its variability: Evidence and mechanisms. *Astron. Astrophys. Rev.* **12**, 273 – 320. doi:10.1007/s00159-004-0024-1.

Garcia, R.R.: 2010, Solar surprise? *Nature* **467**, 668 – 669. doi:10.1038/467668a.

Gray, L., Beer, J., Geller, M., Haigh, J.D., Lockwood, M., Matthes, K., Cubasch, U., Fleitmann, D., Harrison, G., Hood, L., Luterbacher, J., Meehl, G.A., Shindell, D.T., van Geel, B., White, W.: 2010, Solar influences on climate. *Rev. Geophys.* **48**, RG4001. doi:10.1029/2009RG000282.

Haigh, J.D.: 2007, The Sun and the Earth's climate. *Living Rev. Solar Phys.* **4**(2). http://www.livingreviews.org/lrsp-2007-2.

Haigh, J.D., Winning, A.R., Toumi, R., Harder, J.W.: 2010, An influence of solar spectral variations on radiative forcing of climate. *Nature* **467**, 696 – 699. doi:10.1038/nature09426.

Harder, J.W., Lawrence, G., Fontenla, J., Rottman, G., Woods, T.: 2005a, The Spectral Irradiance Monitor: Scientific requirements, instrument design, and operation modes. *Solar Phys.* **230**, 141 – 167. doi:10.1007/s11207-005-5007-5.

Harder, J.W., Fontenla, J., Lawrence, G., Woods, T., Rottman, G.: 2005b, The Spectral Irradiance Monitor: Scientific requirements, instrument design, and operation modes. *Solar Phys.* **230**, 169 – 204. doi:10.1007/s11207-005-1528-1.

Harder, J.W., Fontenla, J.M., Pilewskie, P., Richard, E.C., Woods, T.N.: 2009, Trends in solar spectral irradiance variability in the visible and infrared. *Geophys. Res. Lett.* **36**, 7801. doi:10.1029/2008GL036797.

Harder, J.W., Thuillier, G., Richard, E.C., Brown, S.W., Lykke, K.R., Snow, M., McClintock, W.E., Fontenla, J.M., Woods, T.N., Pilewskie, P.: 2010, The SORCE SIM solar spectrum: Comparison with recent observations. *Solar Phys.* **263**, 3 – 24. doi:10.1007/s11207-010-9555-y.

Hoaglin, D., Mosteller, F., Tukey, J.: 1983, *Understanding Robust and Exploratory Data Analysis*, Wiley, New York.

Krivova, N.A., Solanki, S.K., Floyd, L.: 2006, Reconstruction of solar UV irradiance in Cycle 23. *Astron. Astrophys.* **452**, 631 – 639. doi:10.1051/0004-6361:20064809.

Krivova, N.A., Solanki, S.K., Unruh, Y.: 2011, Towards a long-term record of solar total and spectral irradiance. *J. Atmos. Solar-Terr. Phys.* **73**, 223 – 234. doi:10.1016/j.jastp.2009.11.013.

Krivova, N.A., Solanki, S.K., Fligge, M., Unruh, Y.C.: 2003, Reconstruction of solar total and spectral irradiance variations in Solar Cycle 23: Is solar surface magnetism the cause? *Astron. Astrophys.* **399**, L1 – L4.

Krivova, N.A., Solanki, S.K., Wenzler, T., Podlipnik, B.: 2009, Reconstruction of solar UV irradiance since 1974. *J. Geophys. Res.* **114**, D00I04. doi:10.1029/2009JD012375.

Kurucz, R.: 1993, ATLAS9 Stellar Atmosphere Programs and 2 km/s grid. ATLAS9 Stellar Atmosphere Programs and 2 km/s grid. Kurucz CD-ROM No. 13. Cambridge, Mass.: Smithsonian Astrophysical Observatory, 1993. **13**.

Lean, J.L.: 2000, Evolution of the Sun's spectral irradiance since the Maunder Minimum. *Geophys. Res. Lett.* **16**, 2425 – 2428.

Lean, J.L., Rottman, G.J., Kyle, H.L., Woods, T.N., Hickey, J.R., Puga, L.C.: 1997, Detection and parameterization of variations in solar mid- and near-ultraviolet radiation (200 – 400 nm). *J. Geophys. Res.* **102**, 29939 – 29956.

Lean, J., Rottman, G., Harder, J., Kopp, G.: 2005, SORCE contributions to new understanding of global change and solar variability. *Solar Phys.* **230**, 27 – 53. doi:10.1007/s11207-005-1527-2.

Lockwood, M., Bell, C., Woollings, T., Harrison, R.G., Gray, L.J., Haigh, J.D.: 2010, Top-down solar modulation of climate: Evidence for centennial-scale change. *Environ. Res. Lett.* **5**(3), 034008. doi:10.1088/1748-9326/5/3/034008.

Pagaran, J., Weber, M., Burrows, J.: 2009, Solar variability from 240 to 1750 nm in terms of facular brightening and sunspot darkening from SCIAMACHY. *Astrophys. J.* **700**, 1884 – 1895. doi:10.1088/0004-637X/700/2/1884.

Pagaran, J.A., Harder, J.W., Weber, M., Floyd, L.E., Burrows, J.P.: 2011, Intercomparison of SCIAMACHY and SIM vis-IR irradiance over several solar rotational timescales. *Astron. Astrophys.* **528**, A67. doi:10.1051/0004-6361/201015632.

Rottman, G.: 2006, Measurement of total and spectral solar irradiance. *Space Sci. Rev.* **125**, 39 – 51. doi:10.1007/s11214-006-9045-6.

Rottman, G., Mount, G., Lawrence, G., Woods, T., Harder, J., Tournois, S.: 1998, Solar spectral irradiance measurements: Visible to near-infrared regions. *Metrologia* **35**, 707 – 712. doi:10.1088/0026-1394/35/4/82.

Skupin, J., Noël, S., Wuttke, M.W., Gottwald, M., Bovensmann, H., Weber, M., Burrows, J.P.: 2005a, SCIAMACHY solar irradiance observation in the spectral range from 240 to 2380 nm. *Adv. Space Res.* **35**, 370 – 375. doi:10.1016/j.asr.2005.03.036.

Skupin, J., Weber, M., Noël, S., Bovensmann, H., Burrows, J.P.: 2005b, GOME and SCIAMACHY solar measurements: Solar spectral irradiance and Mg II solar activity proxy indicator. *Mem. Soc. Astron. Ital.* **76**, 1038 – 1041.

Solanki, S.K., Krivova, N.A.: 2004, Solar irradiance variations: from current measurements to long-term estimates. *Solar Phys.* **224**, 197 – 208. doi:10.1007/s11207-005-6499-8.

Solanki, S.K., Unruh, Y.C.: 1998, A model of the wavelength dependence of solar irradiance variations. *Astron. Astrophys.* **329**, 747 – 753.

Thuillier, G., Floyd, L., Woods, T.N., Cebula, R., Hilsenrath, E., Hersé, M., Labs, D.: 2004, Solar irradiance reference spectra. *Geophys. Monogr.* **41**, 171 – 194. doi:10.10219/141GM13.

Tobiska, W.K., Bouwer, S.D.: 2006, New developments in SOLAR2000 for space research and operations. *Adv. Space Res.* **37**, 347 – 358. doi:10.1016/j.asr.2005.08.015.

Tobiska, W.K., Woods, T., Eparvier, F., Viereck, R., Floyd, L., Bouwer, D., Rottman, G., White, O.R.: 2000, The SOLAR2000 empirical solar irradiance model and forecast tool. *J. Atmos. Solar-Terr. Phys.* **62**, 1233 – 1250. doi:10.1016/S1364-6826(00)00070-5.

Unruh, Y.C., Solanki, S.K., Fligge, M.: 1999, The spectral dependence of facular contrast and solar irradiance variations. *Astron. Astrophys.* **345**, 635 – 642.

Unruh, Y.C., Solanki, S.K., Fligge, M.: 2000, Modelling solar irradiance variations: Comparison with observations, including line-ratio variations. *Space Sci. Rev.* **94**, 145 – 152.

Unruh, Y.C., Krivova, N.A., Solanki, S.K., Harder, J.W., Kopp, G.: 2008, Spectral irradiance variations: Comparison between observations and the SATIRE model on solar rotation time scales. *Astron. Astrophys.* **486**, 311 – 323. doi:10.1051/0004-6361:20078421.

Viereck, R.A., Puga, L., McMullin, D., Judge, D., Weber, M., Tobiska, W.K.: 2001, The Mg II index: A proxy for solar EUV. *Geophys. Res. Lett.* **28**, 1343 – 1346.

Viereck, R.A., Floyd, L.E., Crane, P.C., Woods, T., Knapp, B.G., Rottman, G., Weber, M., Puga, L.C., DeLand, M.T.: 2004, A composite Mg II index spanning from 1978 to 2003. *Space Weather* **2**, S10005.

Weber, M., Burrows, J.P., Cebula, R.P.: 1998, GOME Solar UV/vis irradiance measurements between 1995 and 1997 – first results on proxy solar activity studies. *Solar Phys.* **177**, 63 – 77.

Wenzler, T., Solanki, S.K., Krivova, N.A.: 2009, Reconstructed and measured total solar irradiance: Is there a secular trend between 1978 and 2003? *Geophys. Res. Lett.* **36**, L11102. doi:10.1029/2009GL037519.

Wenzler, T., Solanki, S.K., Krivova, N.A., Fröhlich, C.: 2006, Reconstruction of solar irradiance variations in Cycles 21 – 23 based on surface magnetic fields. *Astron. Astrophys.* **460**, 583 – 595. doi:10.1051/0004-6361:20065752.

Willson, R.C., Mordvinov, A.V.: 2003, Secular total solar irradiance trend during Solar Cycles 21 – 23. *Geophys. Res. Lett.* **30**(5), 1199. doi:10.1029/2002GL016038.

Woods, T.N., Rottman, G.J.: 2002, *Solar Ultraviolet Variability over Time Periods of Aeronomic Interest*, *AGU Monogr.* **130**, AGU, Washington, 221 – 234.